GLOBAL PRECIPITATION MEASUREMENT (GPM) MISSION

Algorithm Theoretical Basis Document

Version 1.0

December 1, 2010

Passive Microwave Algorithm Team Facility

TABLE OF CONTENTS

GLOSSARY OF ACRONYMS

A

Advanced Microwave Scanning Radiometer for the Earth observing system (AMSR-E)

Advanced Microwave Sounding Unit (AMSU)

ATBD (Algorithm Theoretical Basis Document)

D

Dual Frequency Radar (DFR)

E

European Centre for Medium-Range Weather Forecasts (ECMWF)

G

GPM (Global Precipitation Measurement)

GPM Microwave Imager (GMI)

GPM Profiling Algorithm (GPROF)

Global Data Assimilation System (GDAS)

Ground Validation (GV)

L

Land Surface Model (LSM)

N

National Centers for Environmental Prediction (NCEP)

Numerical weather prediction (NWP)

P

Precipitation Processing System (PPS)

Passive microwave retrieval (PWR)

Precipitation radar (PR)

T

Brightness temperature (T_b)

Tropical Rainfall Measuring Mission (TRMM)

Tropical Rainfall Measuring Mission - Microwave Imager (TMI)

1.0 INTRODUCTION

1.1 OBJECTIVES

The GPM Mission is an international space network of satellites designed to provide the next generation precipitation observations every two to four hours anywhere around the world. GPM consists of both a defined satellite mission concept and ongoing scientific collaboration involving the global community. The GPM concept centers on the deployment of a "Core" observatory carrying advanced active and passive microwave sensors in a non-Sun-synchronous orbit to serve as a physics observatory to gain insights into precipitation systems and as a calibration reference to unify and refine precipitation estimates from a constellation of research and operational satellites. As a science mission with integrated applications goals, GPM will advance understanding of the Earth's water and energy cycle and extend current capabilities in using accurate and timely information of precipitation to directly benefit the society. The current Algorithm Theoretical Basis Document (ATBD) deals with the Passive Microwave Algorithms associated with the GPM mission. The passive microwave algorithm is designed to take advantage of the Core observatory to define *a-priori* databases of observed precipitation profiles and their associated brightness temperature signals. These databases are then used in conjunction with Bayesian inversion techniques to build consistent retrieval algorithms for each of GPM's constellation satellites. The specific implementation is described below.

1.2 PURPOSE

This ATBD describes the Global Precipitation Measurement (GPM) passive microwave rainfall algorithm, which is a parametric algorithm used to serve all GPM constellation radiometers. The output parameters of the algorithm are enumerated in Table 1. It is based upon the concept that the GPM core satellite, with its Dual Frequency Radar (DPR) and GPM Microwave Imager (GMI), will be used to build a consistent *a-priori* database of cloud and precipitation profiles to help constrain possible solutions from the constellation radiometers.

In particular, this document identifies sources of input data and output from the retrieval algorithm and describes the physical theory upon which the algorithm is based. The document includes implementation details, as well as the assumptions and limitations of the adopted approach. Because the algorithm is being developed by a broad team of scientists, this document additionally serves to keep each developer abreast of all the algorithm details and formats needed to interact with the code. The version number and date of the ATBD will therefore always correspond to the version number and date of the algorithm – even if changes are trivial.

Table 1. Key output parameters from the Level 2 Rainfall Product

Pixel Information		
Parameter	**Units**	**Comments**
Latitude, longitude	Deg.	Pixel position
Surface Type	None	Identifies land/ocean/coast/sea ice
Pixel Status	None	Identifies pixels eliminated by QC procedures
Quality Flag	None	Identified pixels w/o good T_b matches in database
Surface Temperature	K	Likely pass-through through from Model
Land Surface Parameters	None	Ancillary parameters used/retrieved over land
Ocean Surface Parameters	None	Ancillary parameters used/retrieved over ocean
Surface Precipitation	mm/hr	Liquid and Solid Precipitation
Precipitation structure	None	Index for self-similar hydrometeor profiles. 28 layers, separated by hydrometeor species.
Precipitation Diagnostics	None	Type of precipitation and uncertainty
Cloud Water Path	Kg/m^2	Integrated from retrieved profile
Rain Water Path	Kg/m^2	Integrated from retrieved profile
Ice Water Path	Kg/m^2	Integrated from retrieved profile

1.3 SCOPE

This document covers the theoretical basis for the passive microwave algorithm for the retrieval of liquid and solid precipitation from the GMI and GPM constellation radiometers. The GPM radiometer algorithm will be a Bayesian type algorithm. These algorithms search an *a-priori* database of potential rain profiles and retrieve a weighted average of these entries based upon the proximity of the observed T_b to the simulated T_b corresponding to each rain profile. By using the same *a-priori* database of rain profiles, with appropriate simulated T_b for each constellation sensor, the Bayesian method is completely parametric and thus well suited for GPM's constellation approach. The *a-priori* information supplied by GPM's core satellite immediately benefits not just the GMI radiometer but all radiometers that form GPM constellations.

The mathematics of Bayesian inversions are well understood. The solution provides a mean rain rate as well as its uncertainty. The major sources of systematic errors in these algorithms are the quality of the *a-priori* database; the estimate of the forward model uncertainty; and the ancillary information used to subset the *a-priori* database.

Chapter 1 describes the objectives, purpose and scope of the document. Chapter 2 provides satellite instrumentation background details. The process concepts and algorithm descriptions for the geophysical parameters of the Rainfall Product are presented in Chapter 3. Chapter 4 describes the algorithm infrastructure, while chapter 5 summarizes the assumptions and limitations and chapter 6 discusses the various planned algorithm improvements.

1.4 CHANGES FROM PREVIOUS VERSIONS

This ATBD represents version 1.0 and thus the initial ATBD

2.0 INSTRUMENTATION

2.1 GPM CORE SATELITE

The GPM Core Spacecraft will fly two precipitation instruments: the GPM Microwave Imager (GMI) and the Dual-frequency Precipitation Radar (DPR). Together, these instruments will provide a unique capability for measuring precipitation falling as light rain or snow—conditions that have been difficult to detect using previous instruments. Compared to the earlier generation of instruments, the new capabilities of the GMI and DPR are enabled by the addition of high frequency channels (165.6 and 183.3 GHz) on the GMI, and the inclusion of a Ka-band (35.5 GHz) radar on the DPR.

2.1.1 GPM Microwave Imager

GMI - The GPM GMI instrument is a multi-channel, conical-scanning, microwave radiometer serving an essential role in the near-global-coverage and frequent-revisit-time requirements of GPM (see Figure 1). The instrumentation enables the Core spacecraft to serve as both a 'precipitation standard' and as a 'radiometric standard' for the other GPM constellation members. The GMI is characterized by thirteen microwave channels ranging in frequency from 10 GHz to 183 GHz. In addition to carrying channels similar to those on the Tropical Rainfall Measuring Mission (TRMM) Microwave Imager (TMI), the GMI carries four high frequency, millimeter-wave, channels about 166 GHz and 183 GHz. With a 1.2 m diameter antenna, the GMI will provide significantly improved spatial resolution over TMI. Launch date for the core spacecraft: July 21, 2013. Launch date for the low-inclination spacecraft: November, 2014.

Table 2. GMI performance characteristics

Frequency (GHz)	Polarization	NEDT/ Reqmt (K)	Expected* NEDT	Expected Beam Efficiency (%)	Expected Calibration Uncert.	Resolution (km)
10.65	V/H	0.96	0.96	91.4	1.04	26
18.7	V/H	0.84	0.82	92.0	1.08	15
23.8	V	1.05	0.82	92.5	1.26	12
36.5	V/H	0.65	0.56	96.6	1.20	11
89.0	V/H	0.57	0.40	95.6	1.19	6
165.5	V/H	1.5	0.81	91.9	1.20	6
183.31±3	V	1.5	0.87	91.7	1.20	6
183.31±7	V	1.5	0.81	91.7	1.20	6

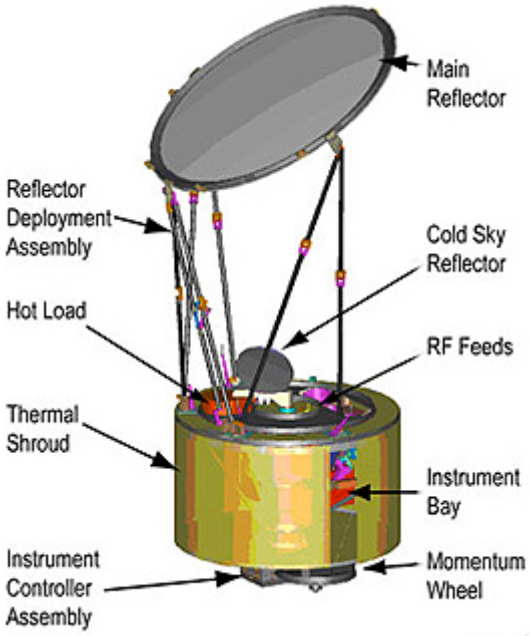

Figure 1. GMI instrument

2.1.2 Dual-frequency Precipitation Radar

DPR - One of the prime instruments for the GPM Core Observatory is called the Dual-frequency Precipitation Radar (DPR). The DPR consists of a Ku-band precipitation radar (KuPR) and a Ka-band precipitation radar (KaPR). The KuPR (13.6 GHz) is an updated version of the highly successful unit flown on the TRMM mission. The KuPR and the KaPR will be co-aligned on the GPM spacecraft bus such that that the 5 km footprint location on the earth will be the same. Data collected from the KuPR and KaPR units will provide the 3-dimensional observation of rain and will also provide an accurate estimation of rainfall rate to the scientific community. The DPR instrument will be allocated 190 Kbps bandwidth over the 1553B spacecraft data bus. The collection of the DPR data will be transmitted to the ground using the TDRSS multiple access (MA) and single access (SA) services.

The DPR is a space borne precipitation radar capable of making accurate rainfall measurements. The DPR is expected to be more sensitive than its TRMM predecessor especially in the measurement of light rainfall and snowfall in the high latitude regions. Rain/snow determination is expected to be accomplished by using the differential attenuation between the Ku-band and the Ka-band frequencies. The variable pulse repetition frequency (VPRF) technique is also expected to increase the number of samples at each IFOV to realize a 0.2 mm/h sensitivity.

The KuPR and KaPR, together with GMI, are the primary instruments on the GPM spacecraft. These Earth-pointing KuPR and KaPR instruments will provide rain sensing over both land and ocean, both day and night. Top-level general design specifications are as follows:

Table 3. DPR performance characteristics

Item	Swath Width (km)	Range Resolu-tion (m)	Spatial Resolu-tion (km Nadir)	Beam Width (deg)	Trans-mitter (SSA)	Peak Transmit Power (W)	Pulse Repe-tition Freq. (Hz)	Pulse Width	Beam #
KuPR	245	250	5	0.71	128	1000	4100 - 4400	2; 1.667 µs pulses	49
KaPR	120	250/500	5	0.71	128	140	4100 - 4400	2; 1.667 µs pulses in matched beams 2; 3.234 µs pulses in interlaced scans	49 (25 matched beams and 24 interlaced scans)

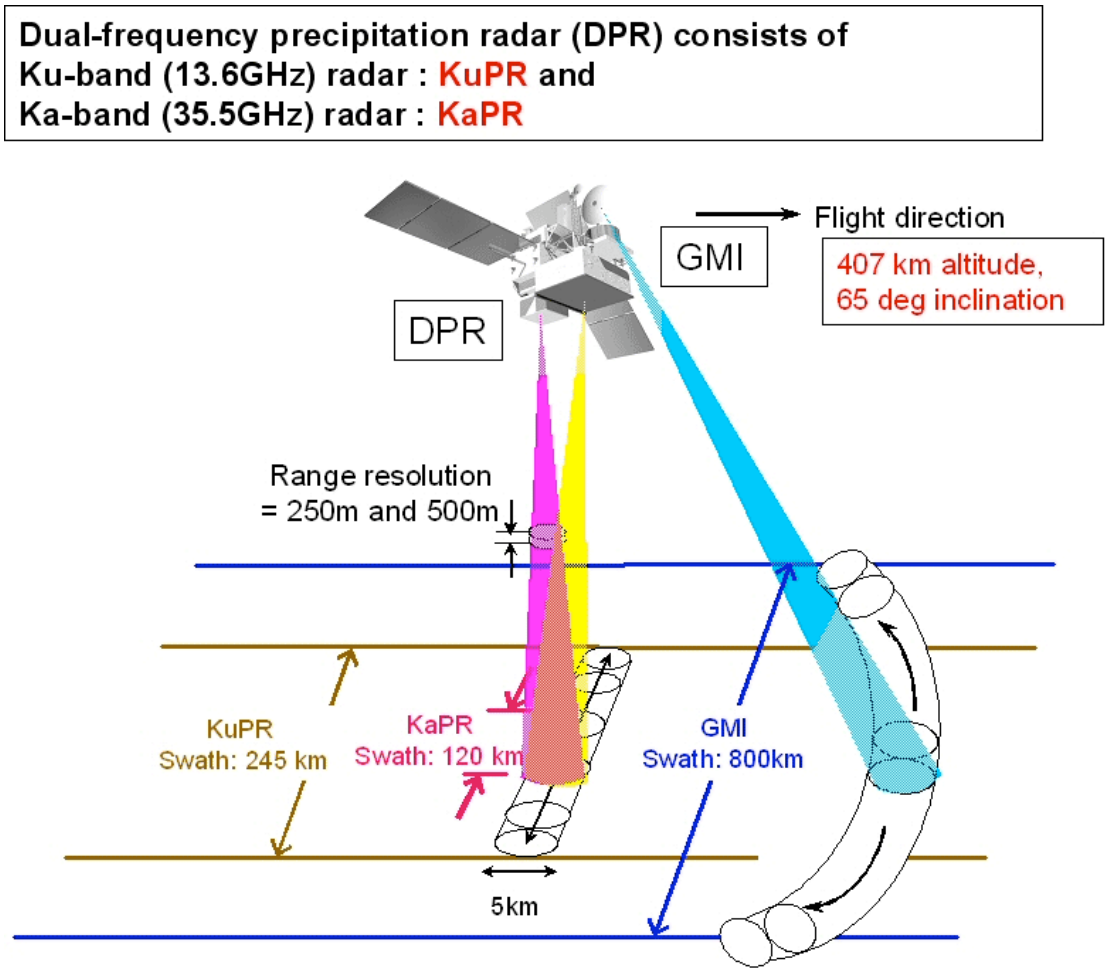

Figure 2. GPM swath measurements

2.2 GPM CONSTELLATION SATELLITES

In addition to the core instruments (GMI and DPR) the passive microwave algorithm will make use of several constellation radiometers that have similar channel sets as the GMI radiometer. These constellation radiometers are listed in Table 4 and described in detail below.

Table 4. Launch and end dates of constellation radiometers in order of launch

Constellation Radiometers	**Launch Date**	**End Date**
AMSR 2	To be determined	N/A
MADRAS	End of 2010	N/A
SAPHIR	End of 2010	N/A
SSMIS	-F-16: Oct. 18, 2003 -F-17: Nov. 4, 2006 -F-18: Oct. 18, 2009	-F-16: Active -F-17: Active -F-18: Active
WindSat	Jan. 6, 2003	Active
AMSR-E	May 4, 2002	Active
*AMSU A AMSU B MHS	-NOAA-15 (NOAAK): May 13, 1998 -NOAA-16 (NOAAL): Sep. 21, 2000 -NOAA-17 (NOAAM): Jun. 24, 2002 -NOAA-18 (NOAAN): Aug. 30, 2005 -MetOp-A: May 21, 2007 -NOAA-19 (NOAAN'): Jun. 02, 2009 -MetOp: 2012	-Active -Active -Active -Active -Active -Active -N/A
ATMS	-NPP: 2011 -JPSS: 2015 -JPSS: 2018	-N/A -N/A -N/A
TMI	Nov. 27, 1997	Active
SSM/I	-F-8: Jun. 20, 1987 -F-10: Dec. 1, 1990 -F-11: Nov. 28, 1991 -F-13: Mar. 24, 1995 -F-14: Apr. 4, 1997 -F-15: Dec. 12, 1999	-F-8: Dec. 1991 -F-10: Nov. 1997 -F-11: May 2000 -F-13: Nov. 2009 -F-14: Aug. 2008 -**F-15: Active

*The AMSU A's and B's have flown together on the 3 NOAA KLM satellites. MHS replaces AMSU-B on NOAA-18 and 19.

**F-15: Beacon corrected data after Aug. 2006.

2.2.1 The Advanced Microwave Scanning Radiometer 2

AMSR 2 – The Advanced Microwave Scanning Radiometer 2 (AMSR 2) which will fly on the GCOM-W1 platform is a sensor to observe microwave radiation at six different frequency bands ranging from 7 GHz to 89 GHz. AMSR 2 is designed to monitor Earth's hydrological cycle including sea surface temperature, cloud water, water vapor, precipitation, sea-ice and soil moisture.

The antenna of the AMSR 2, which receives microwaves from the ground, arc scans the ground surface at a ratio of one turn every 1.5 seconds and observes an area approximately 1,450 kilometers wide in one scan. Using this scanning method, the AMSR 2 can observe over 99 percent of the Earth's area in just 2 days. The diameter of the antenna is about 2 meters, making it the world's largest observation sensor aboard a satellite. The height of the rotating part is about 2.7 meters and the weight is about 250 kilograms. The AMSR 2 can keep rotating such a large and heavy antenna at a speed of one turn per 1.5 seconds for 24 hours a day and more than five years without a minute of rest. Launch date: To be determined.

Table 5. AMSR 2 performance characteristics

Orbit	**Launch**	**Design life (yrs)**	**Local time (LTAN)**	**Swath width (km)**	**Antenna**	**Incidence angle (deg)**
Sun Synchronous with 699.6km altitude (over equator)	JFY201	5	13:30	1450	2.0m offset parabola	Nominal 55

Table 6. AMSR 2 Channel Set

Center Freq. (GHz)	**Bandwidth (MHz)**	**Polarization**	**Beam Width (deg.) (ground res. [km])**	**Sampling Interval (km)**
6.925/7.3	350	V/H	1.8 (35 x 62)	10
6.925/7.3	350	V/H	1.7 (34 x 58)	10
10.65	100	V/H	1.2 (24 x 42)	10
18.7	200	V/H	0.65 (14 x 22)	10
23.8	400	V/H	0.75 (15 x 26)	10
36.5	1000	V/H	0.35 (7 x 12)	10
89.0	3000	V/H	0.15 (3 x 5)	5

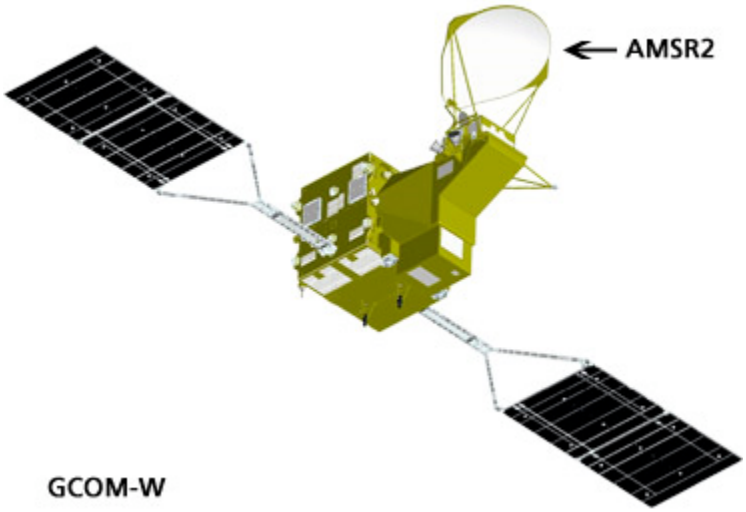

Figure 3. AMSR 2

2.2.2 MADRAS

MADRAS - is a microwave imager, with conical scanning (incidence angle 56°), close to the SSM/I and TMI concepts. The main aim of the mission being the study of cloud systems, a frequency has been added (157 GHz) in order to study the high level ice clouds associated with deep convective systems, and to serve as a window channel relative to the sounding instrument at 183 GHz.

Table 7. Main characteristics of the MADRAS channels

Frequencies	**Polarization**	**Pixel size (km)**	**Main use**
18.7 GHz ± 100 MHz	H/V	40	ocean rain and surface wind
23.8 GHz ± 200 MHz	V	40	integrated water vapor
36.5 GHz ± 500 MHz	H/V	40	cloud liquid water
89 GHz ± 1350 MHz	H/V	10	convective rain areas
157 GHz ± 1350 MHz	H/V	6	cloud top ice

The main uses given here are only descriptive. In practice most of the products will be extracted from algorithms combining the different channels information. The resolutions are those expected in the different channels, accounting for the specification of 10 km given for the 89 GHz channel.

The general Geometry of scanning of the three instruments of the mission is represented in Figure 4.

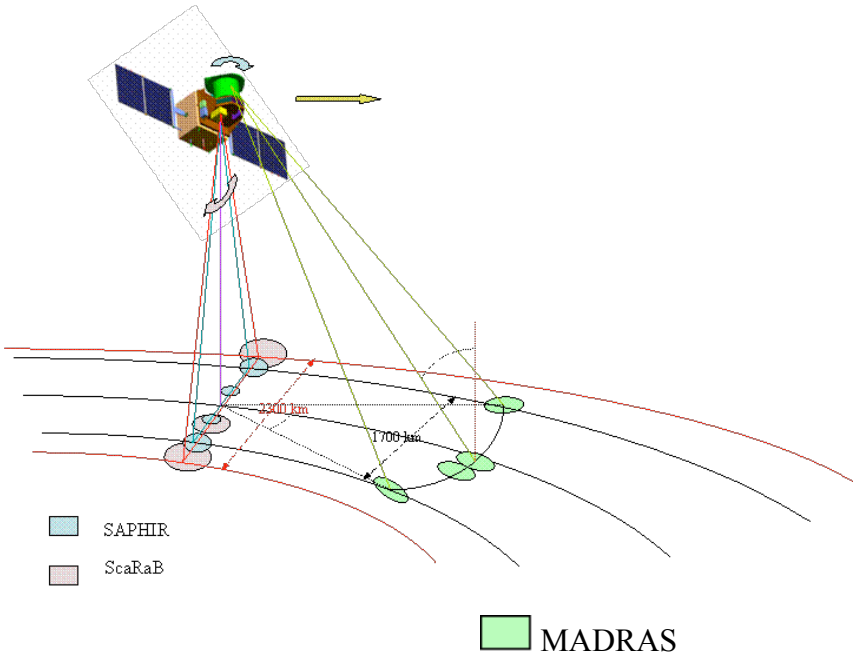

Figure 4. General configuration of the swath of the three instruments of Megha-Tropiques. Size of the footprints has been enhanced in order to show their geometric behavior.

Spectral characteristics include three instruments that compose the core payload of the mission: a microwave imager, a microwave water vapor sounder, a radiative budget radiometer. Preliminary studies have defined the main characteristics of these instruments. Launch date: Scheduled for the second half of 2010.

2.2.3 Sondeur Atmosphérique du Profil d'Humidité Intertropicale par Radiométrie

SAPHIR – Sondeur Atmosphérique du Profil d'Humidité Intertropicale par Radiométrie (SAPHIR) is a sounding instrument with 6 channels near the absorption band of water vapor at 183 GHz. These channels provide relatively narrow weighting functions from the surface to about 10 km, allowing retrieving water vapor profiles in the cloud free troposphere. The scanning is cross-track, up to an incidence angle of 50°. The resolution at nadir is of 10 km.

The atmospheric opacity spectrum (see figure 5) shows a first water vapor absorption line centered at 22.235 GHz, and a second one at 183.31 GHz (pure rotation line). Between these two lines, the water vapor continuum slowly increases absorption by the atmosphere with frequency. The first water vapor line is too low to permit profiling, and its partial transparency is used to obtain the total columnar content. The second line is high enough to enable sounding in the first 10 - 12 km of the atmosphere. The sounding principle consists of selecting channels at different frequencies inside the absorption line, in order to obtain a maximal sensitivity to humidity at different heights. Previous microwave sounders are SSMT2 and AMSU-B, which are operational instruments and

have 3 channels within the 183.31 GHz absorption line (at ±1, ±3 and ±7 GHz), and two window channels, at 150 and 89 GHz. These additional channels give information on the surface and near surface.

Table 8. Channel selection for SAPHIR on board Megha/Tropiques

Channel	Center Freq. (GHz)	Bandwidth (MHz)	Sensitivity (K)	Polarization
S1	183.31±0.2	200	1.82	H
S2	183.31±1.1	350	1.01	H
S3	183.31±2.7	500	0.93	H
S4	183.31±4.0	700	0.88	H
S5	183.31±6.6	1200	0.81	H
S6	183.31±11.0	2000	0.73	H

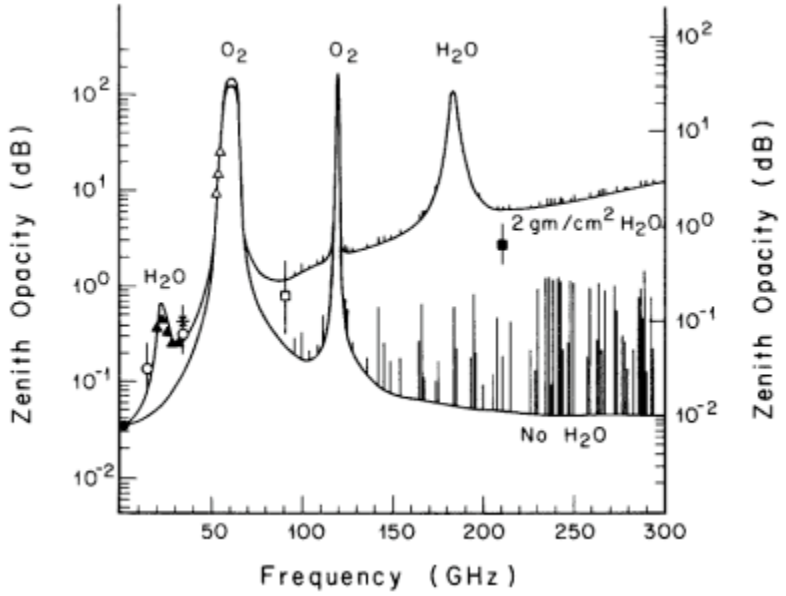

Figure 5. The atmospheric opacity for a US standard atmosphere

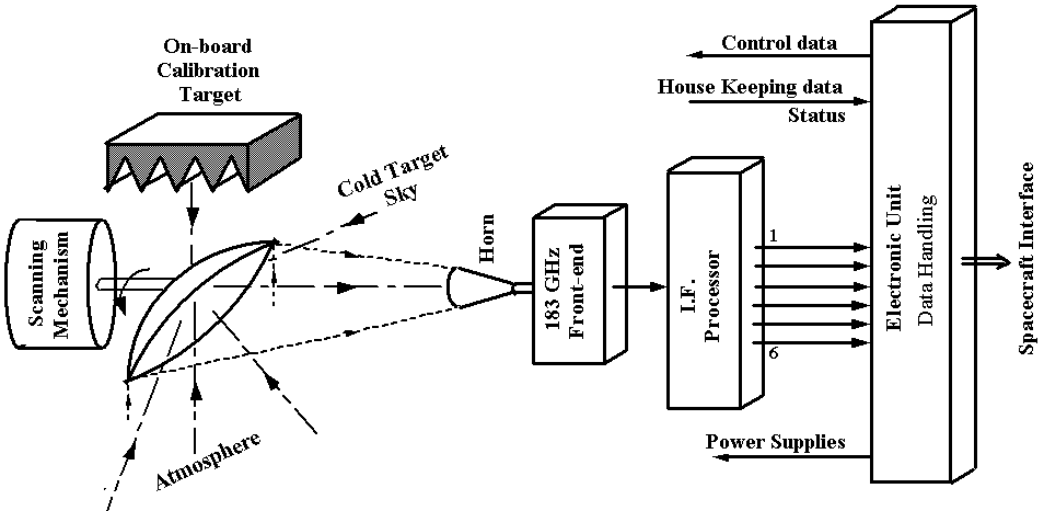

Figure 6. SAPHIR instrument

2.2.4 Special Sensor Microwave Imager/Sounder

SSMIS - The Special Sensor Microwave Imager/Sounder (SSMIS) is a conically scanning passive microwave radiometer with a 53.1 degree Earth incidence angle sensing upwelling microwave radiation at 24 channels covering a wide range of frequencies from 19 - 183 GHz. The Level 1C dataset contains only 11 of these channels, which are most relevant to sensing precipitation. Data is collected along an active scan of 144 degrees across track producing a swath width on the ground of 1707 km. The first of five sensors were launched on board DMSP F16 on October 18, 2003. The SSMIS is a joint US Air Force/Navy multi-channel passive microwave sensor that combines and extends the imaging and sounding capabilities of three separate DMSP microwave sensors including the SSM/T, SSM/T2, and SSM/I. It was built by Northrup-Grumman Electronic Systems.

Table 9. SSMIS characteristics (Note: The channels in the Level 1C dataset are a subset of the full SSMIS channel complement)

Center Freq. (GHz)	**Polarization**	**Bandwidth (MHz)**	**IFOV (km x km)**	**Spatial Sampling (km x km)**	**Sensitivity (K)**
19.35	V/H	350	73x47	45x74	0.35
22.235	V	410	73x47	45x74	0.45
37.0	V/H	160	41x31	28x45	0.22
91.665	V/H	1410	14x13	13x16	0.19
150	H	1640	14x13	13x16	0.53
183.311 +- 1	H	510	14x13	13x16	0.38
183.311 +- 3	H	1020	14x13	13x16	0.39
183.311 +- 7	H	1530	14x13	13x16	0.56

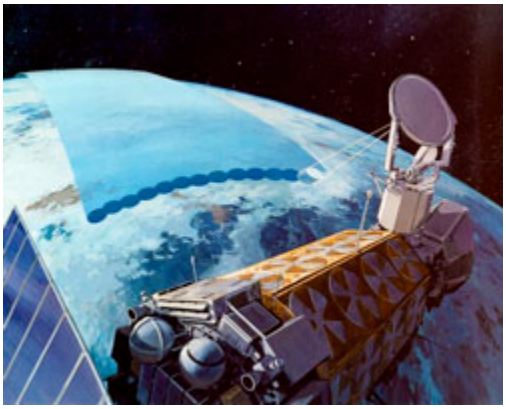
Figure 7. SSMIS

2.2.5 WindSat

WindSat – WindSat is a multi-frequency polarimetric microwave radiometer designed to demonstrate the capability of polarimetric microwave radiometry to measure the ocean

surface wind vector from space. It has 22 channels operating at 5 frequencies. All frequencies have both V and H polarizations and three of the channels also have +/-45, left-hand circular and right-hand circular polarizations. The instrument scans both before and after, and while some frequency bands have a swath width greater that 1200 km, the common swath width is approximately 950 km (68 degrees of scan angle) and the aft common swath is 350 km (23 degrees of scan angle). It was launched on board the U.S. Dept. of Defense Coriolis satellite on January 6, 2003 into an 840 km circular sun-synchronous orbit.

Table 10. WindSat performance characteristics

Center Freq. (GHz)	Polarization	Bandwidth (MHz)	Sensitivity (K)	IFOV (km x km)	Earth Incidence Angle (deg)
6.8	V/H	125	0.48	60x40	53.5
10.7	V/H/+-45/L/R	300	0.37	38x25	49.9
18.7	V/H/+-45/L/R	750	0.39	27x16	55.3
23.8	V/H	500	0.55	20x12	53.0
37.0	V/H/+-45/L/R	2000	0.45	13x8	53.0

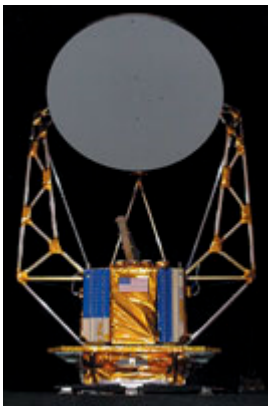

Figure 8. WindSat

2.2.6 Advanced Microwave Scanning Radiometer-E

AMSR-E – The Advanced Microwave Scanning Radiometer-E (AMSR-E) is a conically scanning total power passive microwave radiometer sensing microwave radiation (brightness temperatures) at 12 channels and 6 frequencies ranging from 6.9 to 89.0 GHz. Horizontally and vertically polarized radiation are measured separately at each frequency. There are 2 separate horns at 89 GHz, one being slightly offset from the centerline of the feedhorn array. *(As of 25 October 2004, there are no data from the 89 GHz horn A. The science algorithms have been modified to take this into account).*

The AMSR-E instrument (Figure 10) modified from the design used for the ADEOS-II AMSR, has an offset parabolic reflector 1.6 meters in diameter. Figure 2 shows the Aqua satellite with AMSR-E mounted in front. The atmospheric radiation is focused by the

main reflector into an array of six feedhorns (Figure 9), which then feed the radiation to the detectors

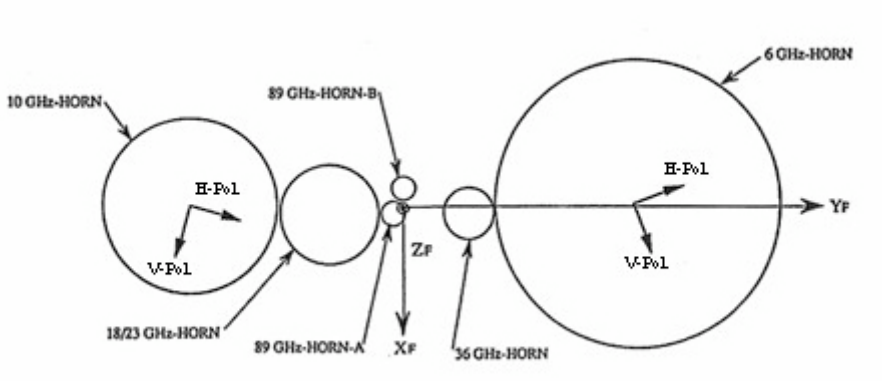

Figure 9. AMSR-E Horn Configuration

A cold load reflector and a warm load are mounted on the transfer assembly shaft and do not rotate with the drum assembly. They are positioned off axis such that they pass between the feedhorn array and the parabolic reflector, occulting it once each scan. The cold load reflector reflects cold sky radiation into the feedhorn array thus serving, along with the warm load, as calibration references for the AMSR-E. Calibration of the radiometers is essential for collection of useful data. Corrections for spillover and antenna pattern effects are incorporated in the data processing algorithms.

The AMSR-E rotates continuously about an axis parallel to the local spacecraft vertical at 40 revolutions per minute (rpm). At an altitude of 705 km, it measures the upwelling scene brightness temperatures over an angular sector of ±61 degrees about the sub-satellite track, resulting in a swath width of 1445 km.

During a period of 1.5 seconds the spacecraft sub-satellite point travels 10 km. Even though the instantaneous field-of-view for each channel is different, active scene measurements are recorded at equal intervals of 10 km (5 km for the 89 GHz channels) along the scan. The half cone angle at which the reflector is fixed is 47.4° which results in an Earth incidence angle of 55.0°. Launch date: May 4, 2002. Table 11 lists the pertinent performance characteristics.

Table 11. AMSR-E performance characteristics

Center Freq. (GHz)	Bandwidth (MHz)	Sensitivity (K)	Mean Spatial Resol-ution (km)	IFOV (km x km)	Sampling Rate (km x km)	Integration Time (m/sec)	Main Beam Efficiency (%)	Beam Width (deg.)
6.925	350	0.3	56	74 x 43	10 x 10	2.6	95.3	2.2
10.65	100	0.6	38	51 x 30	10 x 10	2.6	95.0	1.4
18.7	200	0.6	21	27 x 16	10 x 10	2.6	96.3	0.8
23.8	400	0.6	24	31 x 18	10 x 10	2.6	96.4	0.9
36.5	1000	0.6	12	14 x 8	10 x 10	2.6	95.3	0.4
89.0	3000	1.1	5.4	6 x 4	5 x 5	1.3	96.0	0.18

Figure 10. AMSR-E Instrument

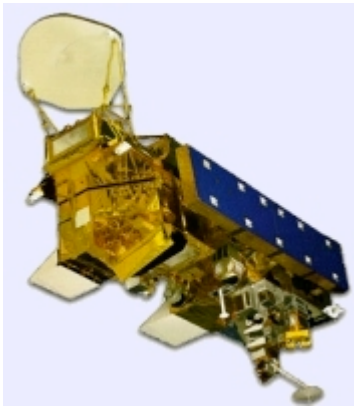

Figure 11. AMSR-E on the Aqua Satellite

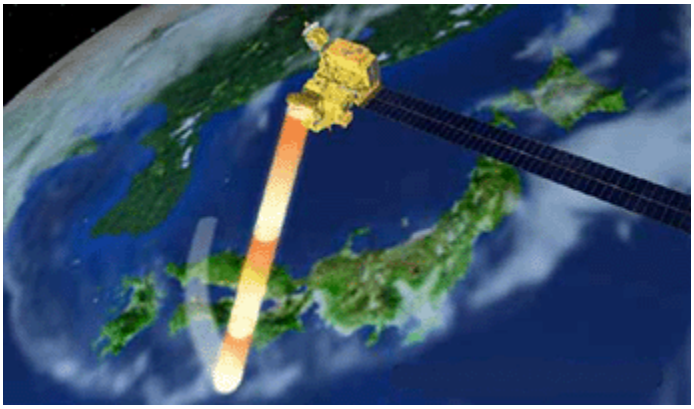

Figure 12. AMSR-E

2.2.7 Advanced Microwave Sounding Unit

AMSU – The Advanced Microwave Sounding Unit (AMSU) is a multi-channel microwave radiometer installed on meteorological satellites. The instrument examines

several bands of microwave radiation from the atmosphere to perform atmospheric sounding of temperature and moisture levels. AMSU data is used extensively in weather prediction. Brightness temperatures are processed as quickly as possible and sent to numerical weather prediction (NWP) centers around the world. This data helps keep the assessment of the current state of the atmosphere correct, which in turn helps make predictions more accurate. Long-term AMSU records are also used in studies of climate.

The AMSU has two sub-instruments, AMSU-A and AMSU-B. AMSU-A has 15 channels between 23.8 and 89 GHz, and is used primarily for measuring atmospheric temperatures (known as "temperature sounding"). It has a ground resolution near nadir of 45 km. AMSU-B, with five channels between 89 and 183.3 GHz, has a spatial resolution near nadir of 15 km and is primarily intended for moisture sounding. Spot size of both sub-instruments becomes larger and more elongated toward the edges of the swath. When the two instruments are used together, there are roughly 9 AMSU-B fields-of-view in a 3x3 array corresponding to each AMSU-A field-of-view. This reflects the higher spatial variability of water vapor compared to temperature. HIRS/3 infrared sounders with the same spatial resolution as AMSU-B are also included on NOAA 15-17 satellites and are used together with AMSU-A and AMSU-B. Together the three instruments form ATOVS, the Advanced TIROS Operational Vertical Sounder.

The Aqua and MetOp AMSU-A instruments are 15-channel microwave sounders designed primarily to obtain temperature profiles in the upper atmosphere (especially the stratosphere) and to provide a cloud-filtering capability for tropospheric temperature observations. The EOS AMSU-A is part of a closely coupled triplet of instruments that include the AIRS and HSB. The MetOp AMSU-A similarly works with HIRS, IASI, and MHS. MHS and HSB are variants on AMSU-B.

Table 12. Radiometric characteristics of the AMSU-A

Channel	**Freq. (GHz)**	**Polarization (at nadir)**	**Band #**	**Sensitivity (K)**	**Primary Function**
1	23.8	V	1	0.30	Water vapor burden
2	31.4	V	1	0.30	Water vapor burden
3	50.3	V	1	0.40	Water vapor burden
4	52.8	V	1	0.25	Water vapor burden
5	53.596 ± 0.115	H	2	0.25	Tropospheric Temperature
6	54.4	H	1	0.25	Tropospheric Temperature
7	54.94	V	1	0.25	Tropospheric Temperature
8	55.5	H	1	0.25	Tropospheric Temperature

9	57.290	H	1	0.25	Stratospheric Temperature
10	57.290 ± 0.217	H	2	0.40	Stratospheric Temperature
11	57.290 ± 0.3222 ± 0.048	H	4	0.40	Stratospheric Temperature
12	57.290 ± 0.3222 ± 0.022	H	4	0.60	Stratospheric Temperature
13	57.290 ± 0.3222 ± 0.010	H	4	0.80	Stratospheric Temperature
14	57.290 ± 0.3222 ± 0.0045	H	4	1.20	Stratospheric Temperature
15	89.0	V	1	0.60	Cloud top/snow

Table 13. Radiometric characteristics of the AMSU-B

Channel	**Freq. (GHz)**	**Polarization (at nadir)**	**Band #**	**Sensitivity (K)**
16	89.9 ± 0.9	V	2	0.37
17	150 ± 0.9	V	2	0.84
18	183.31 ± 1.00	V	2	1.06
19	183.31 ± 3.00	V	2	0.70
20	183.31 ± 7.00	V	2	0.60

2.2.8 TRMM Microwave Imager

TMI – The TRMM Microwave Imager (TMI) is a nine-channel passive microwave radiometer based upon the Special Sensor Microwave/Imager (SSM/I), which has been flying aboard the U.S. Defense Meteorological Satellite Program (DMSP) satellites since 1987. The key differences are the addition of a pair of 10.7-GHz channels with horizontal and vertical polarizations and a frequency change of the water vapor channel from 22.235 to 21.3 GHz. This change off the center of the water vapor line was made in order to avoid saturation in the tropical orbit of TRMM. Table 14 presents the performance characteristics of the nine TMI channels. The increased spatial resolution

evident in Table 14 is due to the lower orbit of the TRMM satellite with respect to the DMSP rather than sensor differences.

The TMI antenna is an offset parabola, with an aperture size of 61 cm (projected along the propagation direction) and a focal length of 50.8 cm. The antenna beam views the earth surface with a nadir angle of 498, which results in an incident angle of 52.88 at the earth's surface. The TMI antenna rotates about a nadir axis at a constant speed of 31.6 rpm. The rotation draws a circle on the earth's surface. Only 1308 of the forward sector of the complete circle is used for taking data. The rest is used for calibrations and other instrument housekeeping purposes. From the TRMM orbit, the 130 scanned sector yields a swath width of 758.5 km shown in Figure 14. During each complete revolution (i.e. a scan period of about 1.9 s), the sub-satellite point advances a distance d of 13.9 km. Since the smallest footprint (85.5-GHz channels) size is only 6.9 km (down-track direction) by 4.6 km (cross-track direction), there is a gap of 7.0 km between successive scans. However, this is the only frequency where there is a small gap. For all higher-frequency channels, footprints from successive scans overlap the previous scans. Launch date: 1997, active.

Table 14. TMI performance characteristics

Channel	**Center Freq. (GHz)**	**Polari-zation**	**Bandwidth (MHz)**	**Sensitivity (K)**	**IFOV (km x km)**	**Sampling Interval (km x km)**	**Integr-ation Time (m/sec)**	**Main Beam Effic-iency (%)**	**Beam width (deg)**
1	10.65	V	100	0.63	63 x 37	13.9x9.1	6.6	93	3.68
2	10.65	H	100	0.54	63 x 37	13.9x9.1	6.6	93	3.75
3	19.35	V	500	0.50	30 x 18	13.9x9.1	6.6	96	1.90
4	19.35	H	500	0.47	30 x 18	13.9x9.1	6.6	96	1.88
5	21.3	V	200	0.71	23 x 18	13.9x9.1	6.6	98	1.70
6	37.0	V	2000	0.36	16 x 9	13.9x9.1	6.6	91	1.00
7	37.0	H	2000	0.31	16 x 9	13.9x9.1	6.6	92	1.00
8	85.5	V	3000	0.52	7 x 5	13.9x4.6	3.3	82	0.42
9	85.5	H	3000	0.93	7 x 5	13.9x4.6	3.3	85	0.43

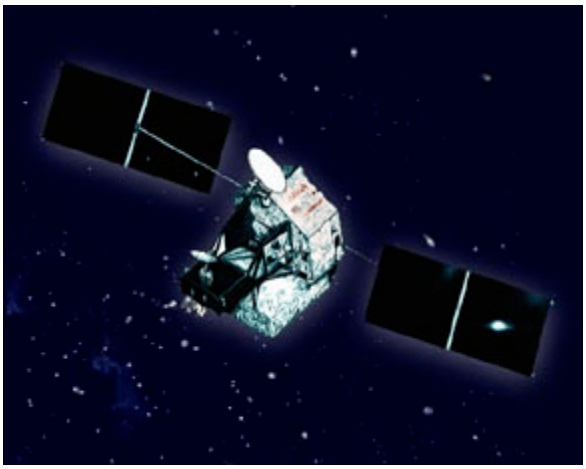

Figure 13. TMI

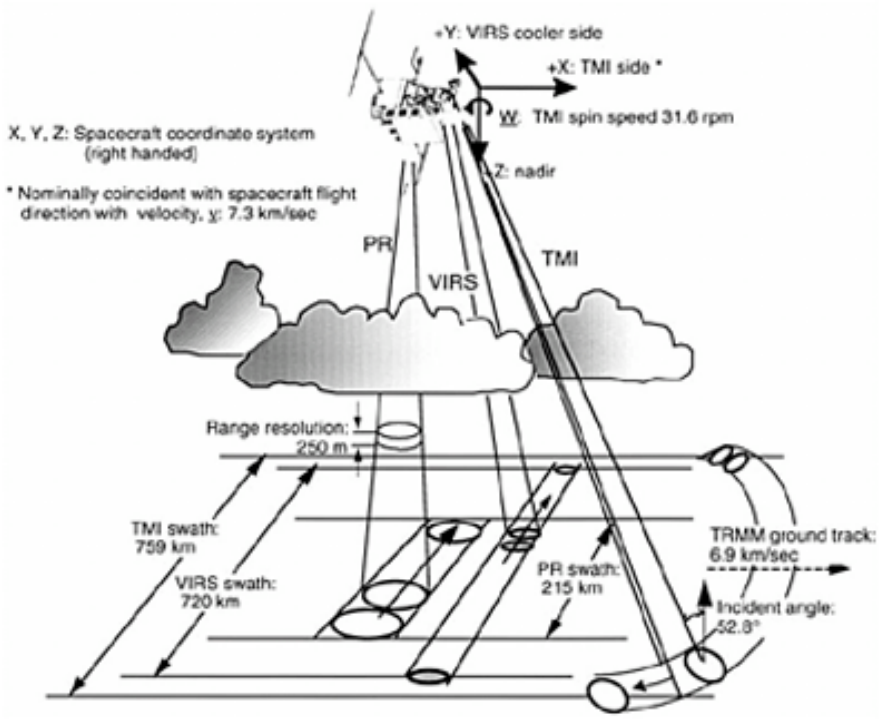

FIG. 1. Schematic view of the scan geometries of the three TRMM primary rainfall sensors: TMI, PR, and VIRS.

Figure 14. Schematic view of the scan geometries of the three TRMM primary rainfall sensors: TMI, PR, and VIRS. Figure provided by Kummerow *et al.* (1998).

2.2.9 Special Sensor Microwave/Imager

SSM/I – The Special Sensor Microwave/Imager (SSM/I) is a seven-channel, four-frequency, linearly polarized passive microwave radiometric system. The instrument measures surface/atmospheric microwave T_bs at 19.35, 22.235, 37.0 and 85.5 GHz. The four frequencies are sampled in both horizontal and vertical polarizations, except the 22 GHz which is sampled in the vertical only.

The SSM/I has been a very successful instrument, superseding the across-track and Dicke radiometer designs of previous systems. Its combination of constant-angle rotary-scanning and total power radiometer design has become standard for passive microwave imagers, (e.g. TRMM Microwave Imager, AMSR). Information within the SSM/I T_bs measurements allow the retrieval of four important meteorological parameters over the ocean: near-surface wind speed (note scalar not vector), total columnar water vapor, total columnar cloud liquid water (liquid water path) and precipitation. However, accurate and quantitative measurement of these parameters from the SSM/I T_bs is a non-trivial task. Variations within the meteorological parameters significantly modify the T_bs. As well as open ocean retrievals, it is also possible to retrieve quantitatively reliable information on sea ice, land snow cover and over-land precipitation.

The instrument is flown onboard the United States Air Force Defense Meteorological Satellite Program (DMSP) Block 5D-2 spacecraft. These are in circular or near-circular

Sun-synchronous and near-polar orbits at altitudes of 833 km with inclinations of 98.8° and orbital periods of 102.0 minutes, each making 14.1 full orbits per day. The scan direction is from the left to the right with the active scene measurements lying ±51.2 degrees about when looking in the F8 forward (F10-F15) or aft (F8) direction of the spacecraft travel. This results in a nominal swath width of 1394 km allowing frequent ground coverage, especially at higher latitudes. All parts of the globe at latitudes greater than 58° are covered at least twice daily except for small unmeasured circular sectors of 2.4° about the poles. Extreme polar regions (> 72° N or S) receive coverage from two or more overpasses from both the ascending and descending orbits each day.

The spin rate of the SSM/I provides a period of 1.9 sec during which the DMSP spacecraft sub-satellite point travels 12.5 km. Each scan 128 discrete, uniformly spaced radiometric samples are taken at the two 85 GHz channels and, on alternate scans, 64 discrete samples are taken at the remaining 5 lower frequency channels. The resolution is determined by the Nyquist limit and the Earth surface's contribution of 3 dB bandwidth of the signal at a given frequency (see Table 15). The radiometer direction intersects the Earth's surface at a nominal incidence angle of 53.1 degrees, as measured from the local Earth normal.

Table 15. Radiometric performance characteristics of the SSM/I (Hollinger 1989)

Center Freq. (GHz)	Polarization	IFOV (km x km)	Spatial Sampling (km)	Sensitivity (K)
19.35	H	69x43	25	0.42
19.35	V	69x43	25	0.45
22.235	V	50x40	25	0.74
37.0	H	37x28	25	0.38
37.0	V	37x28	25	0.37
85.5	H	15x13	12.5	0.73
85.5	V	15x13	12.5	0.69

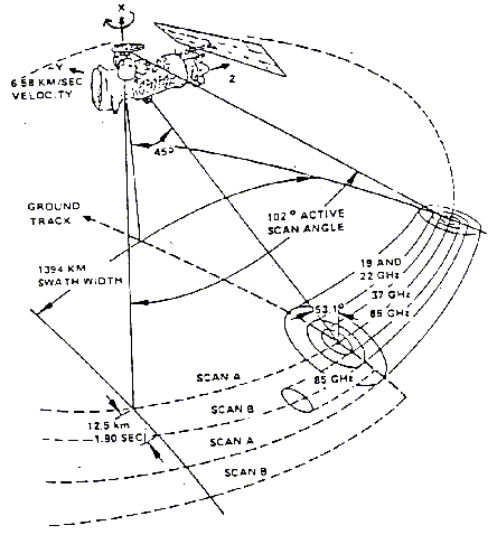

Figure 15. The scan geometry of the SSM/I

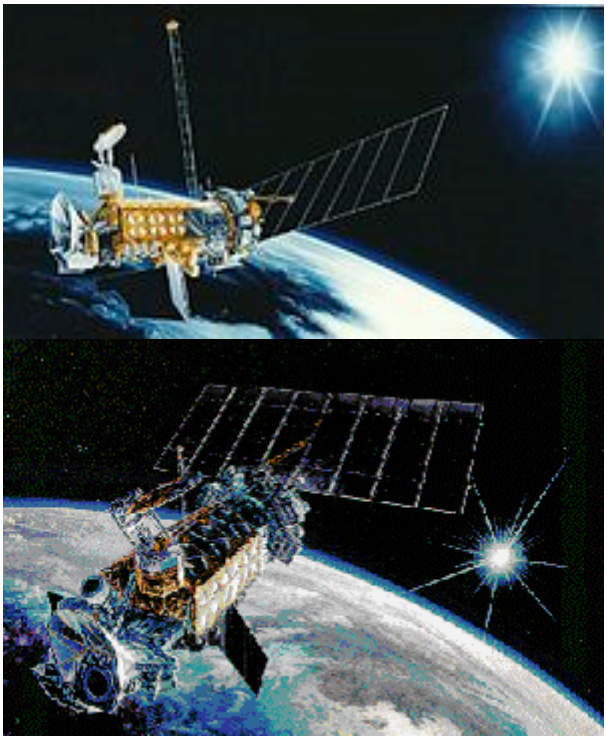
Figure 16. SSM/I

2.2.10 Advanced Technology Microwave Sounder

ATMS – The Advanced Technology Microwave Sounder (ATMS) will operate in conjunction with the Cross-track Infrared Sounder (CrIS) to profile atmospheric temperature and moisture. The ATMS is the next generation cross-track microwave sounder that will combine the capabilities of current generation microwave temperature sounders (Advanced Microwave Sounding Unit – AMSU-A) and microwave humidity sounders (AMSU-B) that are flying on NOAA's Polar Operational Environmental Satellites (POES). The ATMS draws its heritage directly from AMSU-A/B, but with reduced volume, mass and power. The ATMS has 22 microwave channels to provide temperature and moisture sounding capabilities. Sounding data from CrIS and ATMS will be combined to construct atmospheric temperature profiles at 1 degree K accuracy for 1 km layers in the troposphere and moisture profiles accurate to 15 percent for 2 km layers. Higher (spatial, temporal and spectral) resolution and more accurate sounding data from CrIS and ATMS will support continuing advances in data assimilation systems and Numerical Weather Prediction (NWP) models to improve short- to medium-range weather forecasts.

Both CrIS and ATMS (CrIMSS) are selected to fly on the National Polar-orbiting Operational Environmental Satellite System (NPOESS) spacecraft, combining both cross-track infrared and microwave sensors aboard the NPOESS satellite. Expected NPP launch year is 2011.

Table 16. Instrument characteristics of the ATMS

Channel	Center Freq. (GHz)	Bandwidth (GHz)	Center Freq. Stability (MHz)	Temp. Sensitivity (K)
1	23.8	0.27	<10	0.7
2	31.4	0.18	<10	0.8
3	50.3	0.18	<10	0.9
4	51.76	0.4	<5	0.7
5	52.8	0.4	<5	0.7
6	53.596±0.115	0.17	<5	0.7
7	54.4	0.4	<5	0.7
8	54.94	0.4	<10	0.7
9	55.5	0.33	<10	0.7
10	57.290344	0.33	<0.5	0.75
11	57.290344±0.217	0.078	<0.5	1.2
12	57.290344±0.3222±0.048	0.036	<1.2	1.2
13	57.290344±0.03222±0.022	0.016	<1.6	1.5
14	57.290344±0.03222±0.010	0.008	<0.5	2.4
15	57.290344±0.03222±0.0045	0.003	<0.5	3.6
16	88.2	2.0	<200	0.5
17	165.5	3.0	<200	0.6
18	183.31±7	2.0	<30	0.8
19	183.31±4.5	2.0	<30	0.8
20	183.31±3	1.0	<30	0.8
21	183.31±1.8	1.0	<30	0.8
22	183.31±1	0.5	<30	0.9

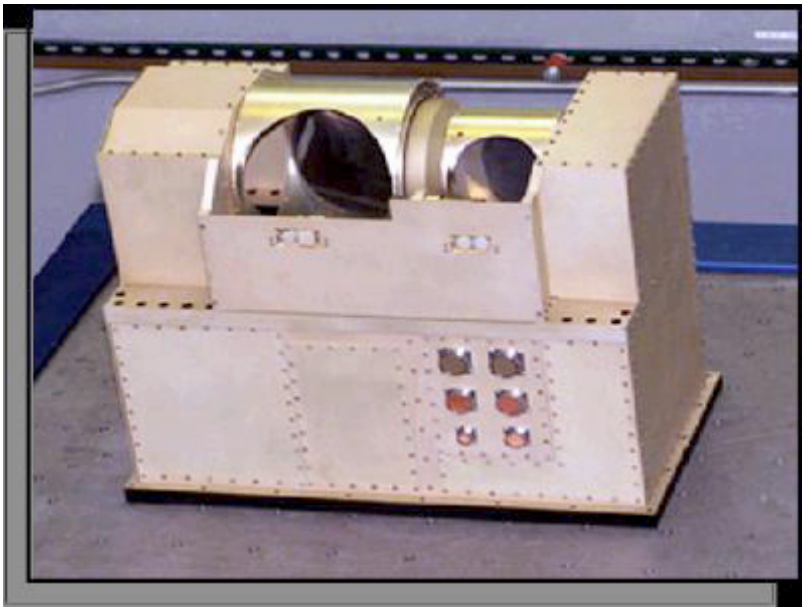

Figure 17. ATMS Instrument

2.2.11 Microwave Humidity Sounder

MHS - The Microwave Humidity Sounder (MHS) is one of the European instruments carried on MetOp-A. MHS is a five-channel, total power, microwave radiometer designed to scan through the atmosphere to measure the apparent upwelling microwave radiation from the Earth at specific frequency bands. Since humidity in the atmosphere (ice, cloud cover, rain and snow) attenuate microwave radiation emitted from the surface of the Earth, it is possible, from the observations made by MHS, to derive a detailed picture of atmospheric humidity with the different channels relating to different altitudes. Temperature at the surface of the Earth can also be determined.

MHS works in conjunction with four of the American instruments provided by the National Oceanic and Atmospheric Administration (NOAA), namely the Advanced Microwave Sounding Unit–A1 (AMSU-A1), the Advanced Microwave Sounding Unit–A2 (AMSU-A2), the Advanced Very High Resolution Radiometer (AVHRR) and the High Resolution Infrared Sounder (HIRS). Along with these instruments, MHS is already in operation on the NOAA-18 satellite, which was launched in May 2005, and it will also form part of the payload on NOAA-N' to be launched in 2008. MHS represents a significant enhancement in performance over the AMSU-B currently flying on the earlier NOAA-15,-16 and -17 satellites.

In conjunction with these American instruments, the MHS instrument will provide improved data for weather prediction models with a resulting improvement in weather forecasting. MHS is intended primarily for the measurement of atmospheric humidity. It will measure cloud liquid water content. Furthermore, it will provide qualitative estimates of precipitation rate.

MHS helps to ensure the continuous and improved availability of operational meteorological observations from polar orbit whilst providing Europe with an enhanced capability for the routine observation of the Earth from space, and in particular, to further increase Europe's capability for long-term climate monitoring.

MHS instrument is a five-channel self-calibrating microwave rotating radiometer on the nadir-facing side of the MetOp-A satellite and is designed to scan perpendicular to the direction flight (across track) at a rate of 2.67 seconds per scan. The swath width of the scan is approximately +/- 50°. The scan is synchronized with the AMSU-A1 and A2 instruments, with MHS performing three scan cycles for every one performed by the AMSU instruments.

The MHS incorporates four receiver chains at 89 GHz, 157 GHz and 190 GHz, with the 183 GHz data sampled in two discrete bands to provide the five channels. The fifth channel is achieved by splitting the 183.311 GHz signal into two channels, each with a different bandwidth.

Table 17. Channel characteristics of the MHS

Channel	Center Freq. (GHz)
1	89.0
2	157.0

3	183.311±1.0
4	183.311 ± 3.0
5	190.31

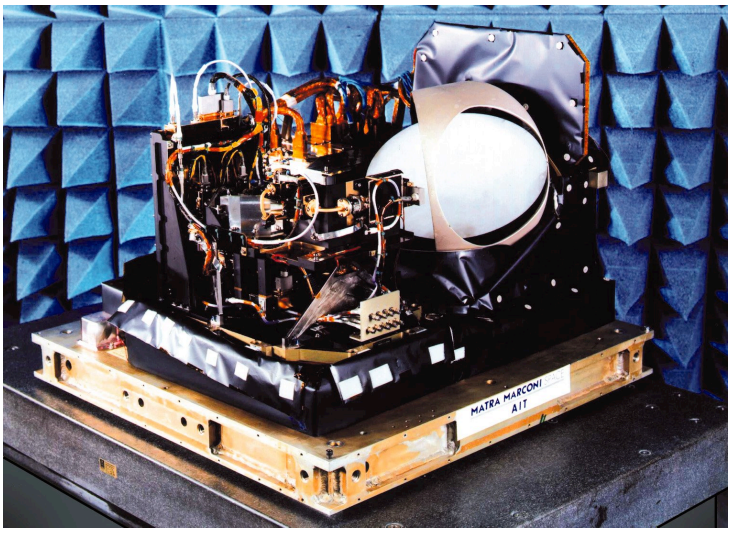

Figure 18. MHS instrument

3.0 ALGORITHM DESCRIPTION

The GPM radiometer algorithm is based upon a Bayesian approach in which the GPM core satellite is used to create an *a-priori* database of observed cloud and precipitation profiles. Once a database of profiles and associated brightness temperatures is established, the retrieval employs a straightforward Bayesian inversion methodology. In this approach, the probability of a particular profile **R**, given $\mathbf{T_b}$ can be written as:

$$\Pr(\mathbf{R} \mid \mathbf{T_b}) = \Pr(\mathbf{R}) \times \Pr(\mathbf{T_b} \mid \mathbf{R}) \qquad (1)$$

where Pr(**R**) is the probability that a certain profile **R** will be observed and Pr($\mathbf{T_b} \mid \mathbf{R}$) is the probability of observing the brightness temperature vector, $\mathbf{T_b}$, given a particular rain profile **R**. The first term on the right hand side of Eq'n (1) is derived from the a-priori database of rain profiles established by the radar/radiometer observing systems discussed in section 3.1. The second term on the right hand side of Eq'n (1), is obtained from radiative transfer computations through the cloud model profiles. The formal solution to the above problem is presented in detail in Kummerow *et al*., (1996). In summary, the retrieval procedure can be said to compose a new hydrometeor profile by taking the weighted sum of structures in the cloud structure database that are radiometrically consistent with the observations. The weighting of each model profile in the compositing procedure is an exponential factor containing the mean square difference of the sensor observed brightness temperatures and a corresponding set of brightness temperatures obtained from radiative transfer calculations through the cloudy atmosphere represented by the model profile. In the Bayesian formulation, the retrieval solution is given by:

$$\hat{E}(R) = \sum_j R_j \frac{\exp\left\{-0.5\left(Tb_o - Tb_s(R_j)\right)^T (O+S)^{-1}\left(Tb_o - Tb_{s(Rj)}\right)\right\}}{\hat{A}} \quad (2)$$

Here, R_j is once again the vector of model profile values from the a-priori database model, Tb_o is the set of observed brightness temperatures, $Tb_s(x_j)$ is the corresponding set of brightness temperatures computed from the model profile R_j. The variables O and S are the observational and model error covariance matrices, respectively, and Â is a normalization factor. The profile retrieval method is an integral version of the well-known minimum variance solution for obtaining an optimal estimate of geophysical parameters from available information (ref. Lorenc, 1986, for a general discussion).

While the mechanics of Bayesian inversions are fairly well understood, three important issues are discussed separately in the following sections. The first is the construction of the a-priori data base itself. Because the data bases constructed for each constellation radiometer are based upon the output of the "combined radar/radiometer" algorithm in GPM, it must be noted that that product cannot be used until after the launch of GPM and sufficient time afterwards to generate a robust data base. As such, the at-launch algorithm will utilize currently available TRMM and CloudSat data to simulate GPM'S DPR radar. Construction of the GPM a-priori databases is detailed in section 3.1. It is broken up into three sub-sections depending upon the level of understanding with regards to the underlying surface. Section 3.1.1 deals with empirical databases that must be constructed when no information is available about the surface. While less than ideal, this is the baseline implementation of the algorithm. Section 3.2 deals with the scenario where the cross-correlations between emissivities at different frequencies is well understood. This allows for more physical retrievals albeit not necessarily of the surface properties themselves. If the emissivity is fully understood in terms of surface geophysical parameters, the rain and cloud profile databases can be integrated with the surface parameters to build more integrated retrievals. This is discussed in section 3.1.3.

If databases are constructed in a completely physical manner as is planned for the integrated retrievals discussed in section 3.1.3, then the process of creating databases for constellation radiometers other than GMI becomes a simple problem in radiative transfer. If, however, we use empirical databases discussed in section 3.1.1, then there is no direct way of computing Tb for the constellation radiometers. The procedures used in this case are described in section 3.2

A separate issue that requires attention is the subsetting of the database. One can always construct databases by latitude, longitude and time of year. This, however, is viewed as a last resort as it does not capture changes in regimes such as ENSO or other expressions of variability in the Earth system. An important step is therefore to select the appropriate a-priori databases in the Bayesian inversion. For instance, ocean pixels will be compared to database entries with similar SST and TPW based upon work done by Berg *et al*. (2006), whereas land, coast, and sea ice pixels are initially compared to database entries of similar latitude, longitude and time of year. The code setup to allow refinements over different surfaces is discussed in section 3.3 while Section 5 lists some of the planned improvements for future versions.

A final issue that the algorithm must deal with is the channels used in the Tb vector defined in Equations 1 and 2. While it is straightforward to assume that all channels will be used, this is not necessarily the case for channels that are sensitive to the surface in cases in which the surface is simply not known (such as coastlines). The approach applied in GPROF2012 is discussed in section 3.4

3.1 THE *A-PRIORI* DATA BASE

3.1.1 The empirical database

The empirical database construction is divided into the individual steps that, in turn, are defined more by historical developments than specific design considerations. The simplest database is the empirical database that can be constructed from the TRMM radar and radiometer. This is section 3.1.1a. This database does not include the 166 and 183 GHZ channels on GPM's GMI instrument. These channels must therefore be added. The method is described in section 3.1.1b. Extra-tropical databases are discussed in section 3.1.1c, while the creation of the databases for HSB and other cross-track sounding radiometers is discussed in section 3.1.1d

3.1.1a – Empirical databases – tropics

As noted in the previous section, the at-launch a-priori database must be created using existing instruments. In the tropics, the database uses existing TRMM PR and TMI sensors. Eleven pixels in the center of the PR swath and the nearest TMI matched footprints define the area used for database construction. The PR liquid and ice water content profiles are calculated for 28 vertical levels using the 2A25 Z-M relationship coefficients and the 2A25 freezing level information. Surface rain rate is also included, and the observed TMI brightness temperatures at each frequency and polarization. Non-raining parameters necessary for radiative transfer calculations but not available from the TRMM data are available and derived from the NASA MERRA (Modern Era Retrospective-Analysis for Research and Applications) reanalysis. The MERRA wind, surface skin temperature, total precipitable water (TPW), and liquid water path (LWP) are interpolated to each of the PR pixels. Observed TMI brightness temperatures are convolved/deconvolved into common footprint sizes, and PR pixel-level quantities averaged over each footprint area.

The observed TMI brightness temperatures are resampled to common fields of view (FOV) corresponding to the 19 and 37 GHz footprints. The resampling technique employed is that of Backus-Gilbert (BG) (1970) as applied to the TMI by Rapp *et al.* (2009). The BG technique uses the observed T_b's of the surrounding pixels to resample the observed T_b at a given scan position as a linear combination of those surrounding T_b's,

$$T_{BG} = \sum_{i=1}^{N} a_i T_{obs}(i),$$

where a_i are coefficients that must be computed for each channel and scan position. In this case an 11x11 array of surrounding T_b's are used for the resampling giving N=121. Because the antenna temperature measurement uncertainties are assumed to be uncorrelated, standard propagation of errors provides the variance in the deconvolved T_b's as

$$e^2 = \left(\Delta T_{RMS}\right)^2 \sum_{1=1}^{N} a_i^2$$

where ΔT_{rms} is the uncertainty in the observed T_b's. Due to the potential for the propagation of large uncertainties, this technique requires a balance between resolution enhancement and amplification of noise. The details describing this process are provided in Rapp *et al.* (2009). Table 18 provides the uncertainty characteristics for the center pixel of the TMI swath for the both the native resolution and the resampled resolutions. Particular care should be taken with the use of the T_b's resampled to the 37 GHz resolution, which has large uncertainties in the low frequency channels.

Table 18. Noise values (e) in [K] at native resolution and computed for TMI T_b's resampled to the 19 and 37 GHz FOV's

Frequency [GHz]	10.65	10.65	19.35	19.35	21.3	37.0	37.0	85.5	85.5
Polarization	V	H	V	H	V	V	H	V	H
e_{native} **[K]**	0.63	0.54	0.50	0.47	0.71	0.36	0.31	0.52	0.93
e_{19} **[K]**	1.61	1.59	0.50	0.47	0.47	0.12	0.11	0.09	0.16
e_{37} **[K]**	3.0	3.0	2.5	2.4	2.4	0.36	0.31	0.2	0.3

The final output files are available on an orbit-by orbit basis via anonymous ftp at rain.atmos.colostate.edu in directory /pub/GPM_Algorthm. The files include geolocation, the non-raining MERRA parameters listed above, as well as the 2A25 water content and rain rate profiles and surface rain rate and freezing level information, observed native TMI T_bs, and convolved/deconvolved T_bs at either the 19 GHz or 37 GHz footprint. The directory includes a simple program for reading the files as well as description of all data fields and formats.

3.1.1b Extension of the tropical empirical databases to include high frequency channels

GMI will carry high frequency channels (centered near 165.5 and 183.3 GHz) in additional to those channels currently available from instruments such as TMI. Because of the large-diameter antenna that GMI will host, upwelling radiance centered on these frequencies will originate from terrestrial surfaces and cloud structures having horizontal spatial scales on the order of 5 km. In order to properly simulate the radiance observed at these higher spatial resolutions, and to partly mitigate the effects of nonlinear radiative transfer (i.e. beamfilling), distributions of high resolution (~5 km) cloud and precipitation

structures are generated through use of a sub-grid scale cloud generator that utilizes the MERRA Reanalysis large-scale average vertical profiles of liquid and frozen cloud hydrometeor contents. Given the grid-average cloud fraction and hydrometeor profiles from MERRA, cloud structures are generated using the maximum/random overlap approximation. It is required that the average cloud fraction and hydrometeor content considering all sub-columns is equivalent to the large-scale MERRA gridbox average. With respect to precipitation structures, liquid and frozen precipitation profiles are also generated for each sub-column. Precipitation profiles are constructed in a sequential manner starting at the highest level at which precipitation is present. At this level, the precipitation is placed in sub-columns where cloud is present (scaled such that the grid-averages are equivalent). At the next lower-altitude level, if the average precipitation is less than or equal to the average at the higher level, the precipitation at the higher level is immediately moved downward to the same sub-columns and scaled lower, if necessary, to match the grid-average. If the average precipitation is greater than the average at the higher level, then the same procedure is followed as before, except that the positive residual is evenly divided over other sub-columns where cloud cover is present. Complete vertical structures of precipitation are generated from top-down in this manner.

Given a distribution of high-resolution cloud and precipitation structures, brightness temperatures for each sub-column are then computed at the GMI frequencies. Since a number of the GMI channels are at different fields-of-view, sub-column brightness temperatures are 'averaged' in such a manner that the spatial resolution associated with the 19 GHz and 85GHZ GMI channels are output.

3.1.1c & d Extra-tropical Combined Active/Passive Database

We will contribute to pre-launch GPM radar-enhanced radiometer algorithm development by creating a database of co-located combined active (CloudSat's Cloud Profiling Radar) and passive (Aqua AMSR-E, Aqua AMSU-A, and NOAA-18 AMSU-A/MHS) T_b observations. The combination of AMSR-E and AMSU-A/MHS will mimic the GMI frequency spectrum, although corrections for viewing angle and/or footprint size will be explored and implemented for the cross-track scanning AMSU-A/MHS instruments. AMSR-E and CloudSat fly in coordinated formation as part of the A-Train constellation, therefore co-locating these observations will not be problematic. Collocations with NOAA-18 AMSU-A/MHS are often possible because Aqua and NOAA-18 orbits frequently overlap. NOAA-18 observations will be matched only when time and distance differences with CloudSat/AMSR-E are within a minimal but yet to be determined, threshold. An initial database spanning one calendar year will be created, although additional years can be processed if deemed necessary. These data will be added to the combined dataset as well if available. Precipitation rate profiles will be derived directly from the CloudSat data using pre-established radar reflectivity factor to precipitation rate relationships for both frozen and liquid hydrometeors. The reflectivity-precipitation rate relationships for frozen hydrometeors will utilize non-spherical ice particle models and a temperature-dependent ice particle size distribution parameterization. First-order attenuation corrections will also be applied to the CloudSat

reflectivity data before converting to precipitation rates. This database will be created globally, but only nominally applied to extra-tropical precipitation due to CloudSat's inherent limitations (e.g. severe attenuation and multiple scattering effects) under heavily precipitating conditions. This database will serve as a placeholder in the radar-enhanced radiometer algorithm until sustained GPM DPR observations are available approximately one year after launch.

3.1.2 Construction of physical databases

A long term SSM/I dataset – Land surface emissivities have been estimated from all available SSMI observations from 1993 to 2008, under clear sky conditions (Prigent *et al*. 1996). The data set has been extensively analyzed and evaluated, by comparisons with both related surface parameters and model outputs. It has been shown to provide robust emissivity calculations, i.e. radiative transfer simulations using the emissivities are closer to the satellite observations. Estimates of the emissivities for all SSMI frequencies are available with a spatial resolution of 0.25°×0.25° at the equator (equal-area grid). It is important to note that this emissivity record needs to be long enough so that the covariance matrices are robust in a statistical sense (this is also important to compute the EOF). Furthermore, the record needs to have wet surface cases (i.e. following a precipitation event) for each location and month, to ensure that the covariance matrices include this variability.

A climatology for SSM/I – From this data set, a monthly-mean climatology at the same spatial resolution has been built. Covariance matrices have been calculated for each location and month. This climatology is the basis of the TELSEM tool used to estimate MW emissivities for other instruments (see section 3.2.2). This climatology will be used to associate each situation in the *a-priori* dataset with an emissivity estimate (or the surface class that will be defined on them).

Validation of the emissivities – In order to validate the emissivity estimates, we have performed comparisons between real observations (AMSU-A, -B, AMSR-E, HSB) and radiative transfer simulations (Aires *et al*. 2010; Aires *et al*. 2010) using various emissivity sources (TELSEM first guess, emissivity retrieval, emissivity model). We believe this is the right way to compare sources, in particular if model emissivities needs to be included later on in the *a-priori* dataset.

There are two alternative solutions to use the emissivity information for the Bayesian proximity search in the *a-priori* dataset: (1) find self-similarity surface classes based on clustering, and (2) use an EOF/PCA representation of the emissivities to reduce the dimension of the Bayesian search space.

Self-Similarity emissivity classes – We have been using a clustering algorithm (K-means or Kohonen methods) in order to classify the surface based on the emissivity information. In Figure 19, the globe is classified into 10 classes for January (Prigent *et al*. 2008). In this example, class 10 is for water-covered pixels, classes 6-9 are for snow/ice-covered

pixels and classes 1 to 5 are for increasing vegetation cover. Using the TELSEM tool, we have analyzed the correlation structure and the covariance matrices for each class, and each pixel location.

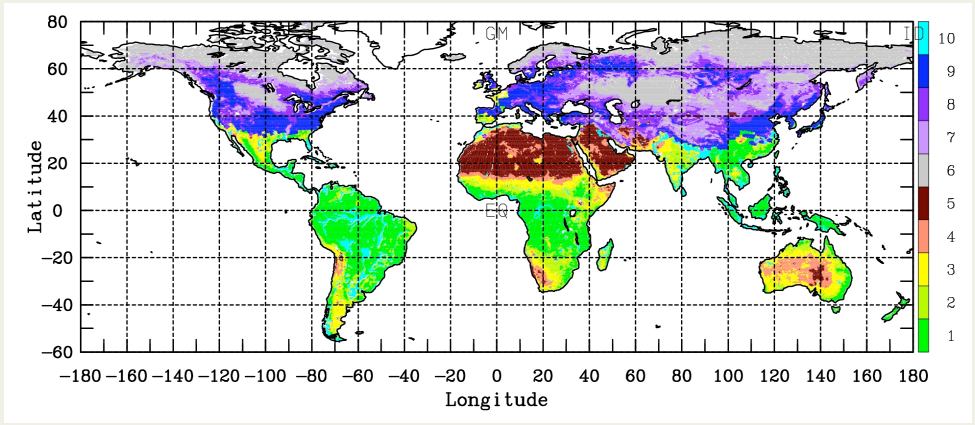

Figure 19. Clustering of the SSM/I classes in 10 self-similar emissivity classes

It is proposed, here, to reproduce such a global classification for each location/month. The goal is to obtain 15/25 classes. We will collaborate with Grant Petty to determine if this classification should be done on emissivity alone or if the covariance matrix should also be taken into account. Various clustering algorithms can be tested. A thorough analysis of each class is necessary, in particular the treatment of the coast and snow/ice pixels. In Figure 20 it is shown that this type of algorithm can be used with the desired number of classes.

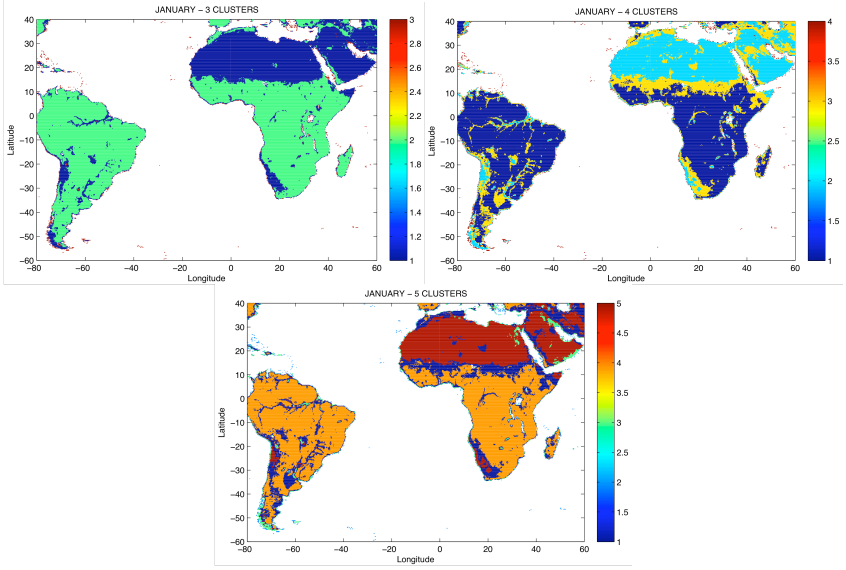

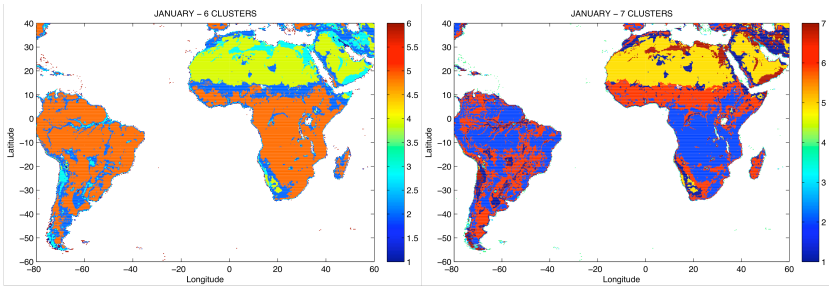

Figure 20. Clustering of surface based on the emissivity information. The number of classes that is desired can be chosen, the number of classes shown here ranges from 3 to 7. Since snow is limited in this experiment, the first 3 classes are arid regions, vegetated areas and coasts.

EOF analysis – The second alternative to use the emissivity information in the Bayesian retrieval algorithm is the EOF representation of the emissivities. Since the covariance matrices are available for each location/month, EOF components can be computed. In Figure 21, the emissivity is reconstructed based on its EOF representation when an increased number of components are used, from 1 EOF to 4 EOFs. It can be seen that the first component provides a good general behavior of the SSM/I emissivities, the vegetated areas and the hydrologic structures are well represented with this unique first EOF. The second EOF represents information on the arid regions. Adding the third component modifies only slightly the emissivity information.

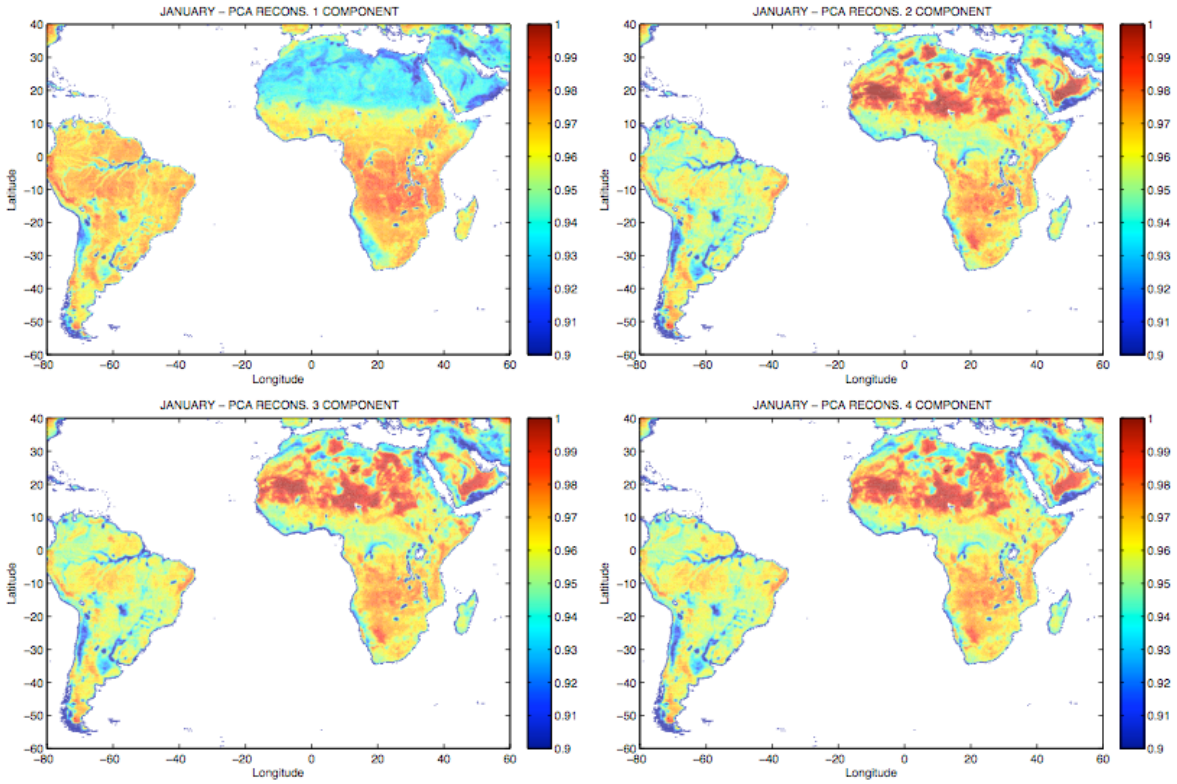

Figure 21. Emissivity maps reconstructed using an increasing number of EOFs, from 1 to 4 components

This is not surprising considering Figure 22 where the percentage of variance explaining the emissivity variations is represented for an increased number of EOFs: the first two components explain already 97% of the emissivity information. This EOF analysis is done over the South-America and African continents, results should be different for a global view when snow will be present.

Figure 22 goes here 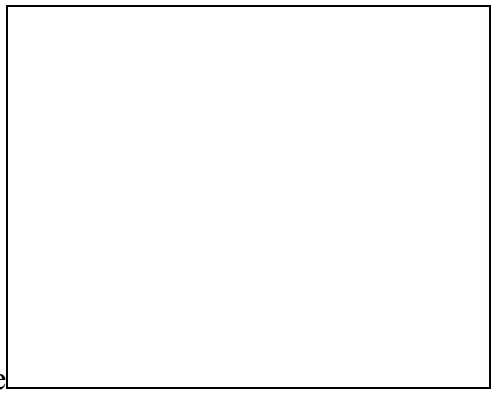

Figure 22. Percentage of emissivity variance explained with an increased number of EOF components

A thorough analysis of these EOFs is necessary. What are the spectral signatures of the EOFs? A discussion with the algorithm team is necessary in order to define which configuration should be used: a global EOF or an EOF for each surface class. We need also to understand the details of the EOF use in the retrieval algorithm: Even if the Bayesian search is done using the EOF, based on the covariance matrices, the mean emissivity is important (you can have two situations with similar covariance matrices and really different mean emissivity).

3.1.3 Construction of integrated databases

Three types of databases will be integrated to provide high resolution, dynamic information to characterize the meteorological, hydrological and radiative states of the global land surface. The three types include:

- Type 1. Static and slowly-varying land surface geophysical parameters, such as land/water boundaries, topography, land cover, vegetation, , and soil properties (Table 19). Most of these datasets can be provided at a base resolution of 1-km to support dynamic foot-printing (Sudradjat *et al*. 2011) as well as to support simulations of land surface physical states and fluxes with Goddard Land Information System (LIS) (see below).

- Type 2. Land surface physical states. Near-real time simulation of dynamic land surface physical states and fluxes (e.g., snow cover, soil moisture, canopy water content and surface temperature) will be routinely produced with LIS. Assuming robust covariance relationships are developed that depend on these dynamic state variables, we can provide footprint-scale estimates of the principal covariance predictors on a nearly-instantaneous basis or, if computational/storage resources require, aggregated to a coarser space/time scale (e.g., daily, 10km). These states are expected to include variables known to be critical for characterizing land surface microwave radiative properties, such as skin temperature, soil moisture and snow cover.

- Type 3. Land surface microwave radiative states. A surface microwave emission model may be employed along with the dynamic land surface states described above, to provide dynamic land surface microwave radiative states, including emissivity and Tb. We currently have the capability to utilize the LIS outputs described above as inputs to the Community Radiative Transfer Model (CRTM), developed at the U.S. Joint Center for Satellite Data Assimilation. CRTM computes land surface emissivity for various surface types using a two-stream radiative approximation (Weng *et al*. 2001). With the support of Type 1 and 2 datasets, LIS/CRTM can routinely produce land surface skin temperature and emissivity at GPM-relevant frequencies and polarizations, especially the dynamic features such as changes of these radiative properties before and after precipitation.

As an example, Figure 23 shows the land surface emissivity for AMSR-E's 12 channels simulated by LIS/CRTM.

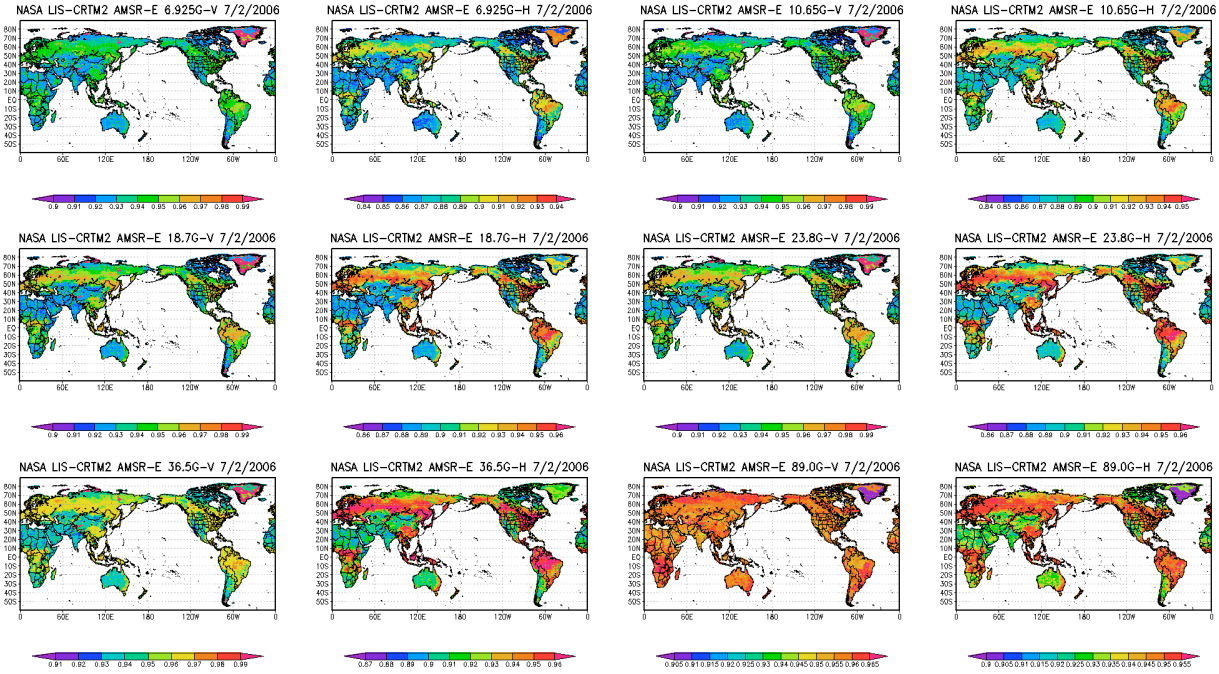

Figure 23. Land surface emissivity modeled with LIS/CRTM over the globe for the 12 channels of AMSR-E, for Jul. 2, 2006

Table 19. Static and semi-static land surface parameters

Id	Name	Native name/format	Native spatial proj./res.	Time res.	Note
1	MODIS C5 Land Cover	Land Cover Type Yearly L3 Global 500m SIN Grid (MCD12Q1.005), HDF-EOS	Sinusoidal grid, MODIS tiles, 500m	Yearly	Two layers of classifications: IGBP and UMD. Mosaic'ed and reprojected to LIS 1km with MODIS Reprojection Tool.
2	MODIS C5 LAI	LAI/FPAR 8-Day L4 Global 1km (MCD15A2.005), HDF-EOS	Sinusoidal grid, MODIS tiles, 1km	8 day	Mosaic'ed and reprojected to LIS 1km with MODIS Reprojection Tool.
3	MODIS C5 Albedo	Albedo 16-Day L3 Global 1km (MCD43B3.005), HDF-EOS	Sinusoidal grid, MODIS tiles, 1km	16 day	Mosaic'ed and reprojected to LIS 1km with MODIS Reprojection Tool. A higher resolution (500m) version is also available (MCD43A3.005)
4	SRTM30 Topography at 1-km	SRTM30, Version_2.1, Binary	Lat/lon grid, 27 SRTM tiles, 30 arc second (1/120 deg)	Static	Reprojected to LIS 1km (1/100 deg) with nearest neighbor.
5	SRTM3 Topography (~90m)	SRTM3, Version_2.1, Binary	Lat/lon grid, 1x1-deg SRTM tiles, 3 arc second (1/1200 deg)	Static	No reprojection done.
6	Global Lakes and Wetlands at 1-km	WWF Global Lakes and Wetlands Database, Binary	Lat/lon grid, global 30 arc second (1/120 deg)	Static	Reprojected to LIS 1km (1/100 deg) with nearest neighbor.
7	Global Soil Texture at 1-km	FAO/STATSGO Merged Soil Texture, Binary	FAO: Lat/lon grid, 5 minute. STATSGO: UTM 1km	Static	Fei Chen's group at NCAR merged the two datasets for their WRF runs.

3.2 CREATING CONSTELLATION DATA BASES

3.2.1 Empirical databases

Translation of empirical algorithms – The initial algorithms for TMI will be generated empirically using TMI and PR data from TRMM for all surfaces except ocean. These will need to be adjusted to for use on GMI and the constellation sensors to account for differences in frequency, view angle and resolution. This is in many ways analogous to

the work of the X-CAL working group except the translations must work in rainy conditions.

The key tool for this translation is the 1DVAR algorithm of Boukabara et al. (Passive Microwave Remote Sensing of Extreme Weather Events Using NOAA-18 AMSUA and MHS, S. Boukabara, F. Weng, Quanhua Liu, IEEE Transactions on Geoscience and Remote Sensing, July 2007, Vol: 45, Issue: 7, Part 2, 2228-2246, DOI: 10.1109/TGRS.2007.898263, or MiRS: An All-Weather 1DVAR Satellite Data Assimilation & Retrieval System, Submitted to IEEE Trans. on Geosc. and Remote Sensing, Under review, 2010). The algorithm, the Microwave Integrated Retrieval System (MiRS), inverts the radiative transfer equation by finding radiometrically appropriate profiles of temperature, moisture, liquid cloud, hydrometeors as well as the surface emissivity spectrum and skin temperature. The inclusion of the cloud and hydrometeor parameters within the inverted state vector make the assimilation/inversion of cloudy and rainy radiances possible and therefore provides an all-weather capable system. MiRS can use radiometric data from the source sensor (e.g. TMI) over a wide variety of conditions including the rainy ones, to compute surface properties and a set of profiles of geophysical variables. These geophysical retrievals can then be used in the Community Radiative Transfer Model (CRTM) to compute synthetic observations for any chosen target sensor, simulating the different sensor frequencies, bandwidths and viewing geometries. The CRTM is developed at the U.S. Joint Center for Satellite Data Assimiliation and is an integral part of the MiRS algorithm. The emissivities and profiles resulting from MiRS can then be used to compute synthetic observations for any chosen target sensor. By saving the emissivities and profiles, the same computations can be used for sensors not defined at the time of the original run.

The results will be subsetted to match the surface types for which the empirical algorithms are defined. Within each subset the mapping of the source and target channels will be derived by fitting the T_b differences to a curve. The scatter in this mapping will be used to estimate the uncertainty of the translation.

The angular and frequency dependence of the surface emissivities can be estimated by examination of the emissivities for various beam positions of the cross track scanners and then interpolating in frequency using the various channels of a given sensor and even using multiple sensors.

Spatial resolution differences can be addressed in two ways. If the source sensor has better resolution than the target sensor, the output of the 1DVAR can simply be smoothed (*i.e.* convolved). If better resolution is needed, a transformation can be generated by comparing histograms of the observed and predicted T_Bs.

3.2.2 Physical databases

TELSEM – A frequency, angular, and polarization dependence of the emissivities have been studied using emissivity estimates for SSM/I, TMI and AMSU instruments (Prigent

et al. 2008). A parameterization of the emissivities under all observing conditions is proposed between 19 and 100GHz. It has been shown that this parameterization can also be applied with benefits down to 6 GHz and up to 183 GHz. A Tool to Estimate Land Surface Emissivities in the Microwaves (TELSEM) has been developed and is being plugged to RTTOV (Aires *et al*. 2010). It provides first guess estimates of the emissivities along with their error covariance matrix, for each land surface point and month. This tool has been made available to the GPM community, in particular to build the GPM simulator.

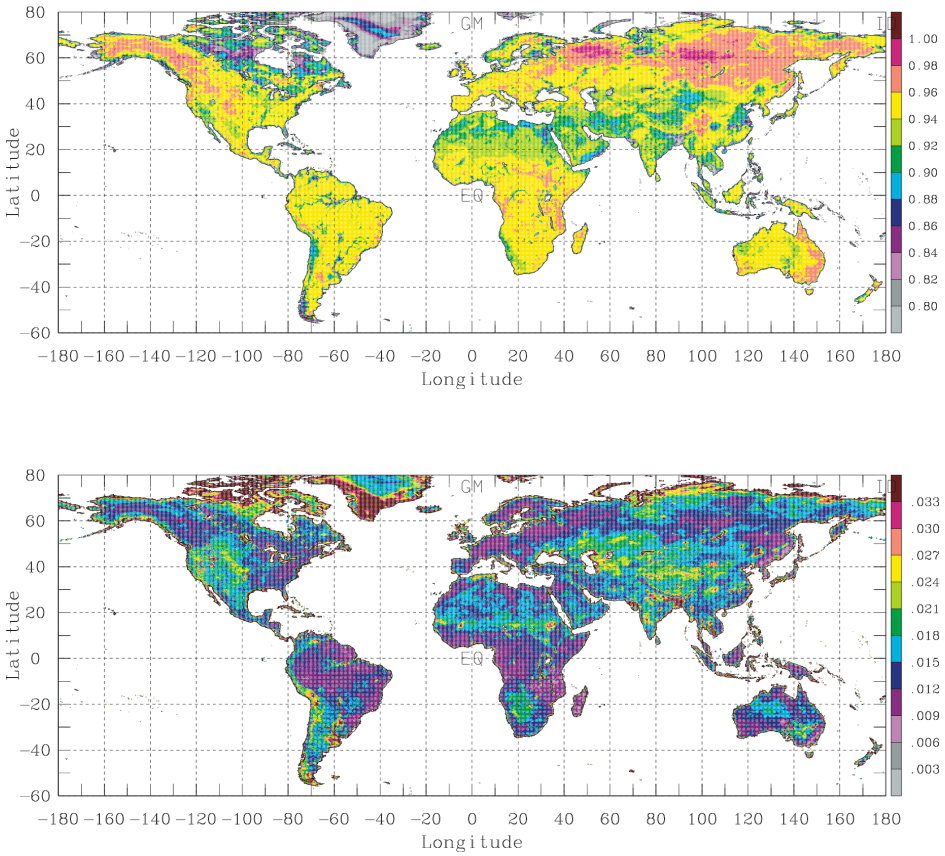

Figure 24. TELSEM emissivity estimate (up) at 31.4 GHz, together with the corresponding emissivity uncertainty (down) from the TELSEM covariance matrices.

Using TELSEM to simulate other emissivity atlases – TELSEM can be used to build emissivity climatologies for the other instruments: GMI, TMI, AMSR-E. The associated covariance matrices can also be generated. We expect to use the same emissivity classes for all the instruments and the SSM/I climatology will be the dataset used for that. But the simulation of emissivities for other instruments is important to associate an emissivity estimate for the *a-priori* dataset in order to perform radiative transfer simulations on them.

Self-Similarity emissivity classes – The classification defined for the SSM/I emissivities will be used for all the other instruments.

EOF analysis – The EOF is not expected to be done on other instruments unless it is convenient for the algorithm team.

Evaluation of surface skin temperature estimates – Surface skin temperature estimates, from re-analyses, surface models, IR observations or microwave measurements show larger differences than expected. Even for a given type of estimate (e.g. satellite IR retrieval), the differences can be significant, especially during the day, in arid and semi arid regions. We have undertaken an evaluation of the different estimates of surface skin temperatures, along with *in situ* measurements, in order to assess the errors associated to each measurement and eventually provide guidance to improve these estimates. We can help the GPM team select Ts estimates that will be compatible with GPM requirements and processing.

3.2.3 Integrated databases

The integrated databases for land surfaces (3.1.3) will be coupled to atmospheric radiative transfer models to predict brightness temperature as observed by GPM. Radiative transfer through the atmosphere can be computed by either CRTM or the Goddard Satellite Data Simulator Unit (G-SDSU).

Integrated databases will initially be constructed for land surfaces that are demonstrated to be well understood and modeled by the procedures detailed in the previous section. These databases will integrate the conribution to the upwelling radiance from the surface with atmospheric profiles in a fully physical representation utilizing the methods detailed for the ocean algorithm. Radiative transfer calculations begin with the surface emissivity modeling, and are performed through the atmosphere. Some background parameters necessary for the radiative transfer – surface temperature for example, can be taken from the land surface models and interpolated with values from radar-matched CRM atmospheric profiles in the same manner as that used by the ocean algorithm. Others will need ancillary data sources. The integrated databases will then contain full surface and atmospheric information and their associated brightness temperatures for use in a Bayesian retrieval scheme.

Over the course of time, as the science progress from several PMM Science Team researchers evolves (i.e., improved emissivity modeling, understanding the temporal variability of snow and arid surfaces, etc.), the procedure will be repeated for more complex surfaces.

3.3 DATABASE SELECTION CRITERIA

The Bayesian scheme used in the retrieval scheme can be thought of as assigning weight for each data base entry to the retrieved pixel. The weight, as in equation 2, is based upon the difference between observed T_b and that corresponding to each database entry. The T_b difference is modulated by the uncertainty in both the observations and the

computed T_b for each entry such that the weight can really be thought of as the T_b difference at each channel normalized by the uncertainty in that channel.

While the Bayesian scheme works without further input, it does become more efficient as well as more accurate if additional information can be supplied that constrains the database profiles that need to be searched. Computationally, it makes sense not to search all database entries whose freezing level might be less than 1 km above the surface – as these would not correspond to tropical cases in the first place. If one searches the entire database for each pixel, the effect is not only a computational slowdown, however, but also an increase in uncertainty as there will always be some pixels whose T_b match sufficiently well to impact the result in some small, but possibly negative way.

The first subset of databases will be done using surface type. We will classify each pixel as Ocean, Land, Coast, sea ice or coast with sea ice. This will be based upon static land surface maps in addition to sea ice extent derived from Reynolds climatology. The databases, however, benefit from a further segregation based upon atmospheric states.

Over oceans, Berg *et al*., (2001) found that SST and TPW led to more self consistent retrieval from the TMI sensor when compared to the TRMM PR data. The combination of these parameters defines the overall temperature and humidity structure of the atmosphere. In the baseline version of the algorithm, we will therefore continue this practice over oceans – using SST and TPW from the MERRA reanalysis in the development changing to the GDAS forecast in order to accommodate real time requirements. Over land, we will use the same approach with LST and TPW. However, land requires a further subset of the database into surfaces with similar emissivities. Initially, when the empirical databases are used, land will be divided according 16 MODIS land surface classification classes. Each class will be divided by time of year (Month±1). Where physical databases are available (i.e. cross correlations among emissivities at different frequencies), we will simultaneously ask for regions that appear self-similar in this space so that databases can be created appropriately. A time tag will likely still be required. Once the algorithm is fully integrated with land surface parameters, these can be accounted for and the databases can once again be subsetted by atmospheric conditions alone.

3.4 CHANNEL SELCTION CRITERIA

Irrespective of whether the *a-priori* database is created using physical or empirical methods, the retrieval itself has only the sensor T_b and ancillary information available in order to select suitable database entries. More channels should, in principle, reduce database entries that are consistent and thus reduce the uncertainties. This, however, may not be true when the surface characteristics are not known (e.g. coastline). In this case, the channels that are sensitive to the surface may simply add noise to the retrieval. Research, labeled as "channel selection criteria" is underway to help define what channels should be used in the retrieval itself. In particular, the research is focused on removing the surface sensitive channels when the surface is unknown.

- Precipitation-free brightness temperature covariance database covering the globe.
    - Initially TMI
    - Extend to AMSR-E
- Suggested procedure for evaluating model-computed emissivities against above empirical co-variances.
- Global algorithm for optimally removing local background noise (including that due to coastlines, as well as temporal and spatial variability of emissivity over land areas) from desired precipitation signature(s), also providing residual noise estimates.
- Attempt to empirically characterize signature of surface snow cover and compare with physical and empirical signatures of precipitation.
- Prototype global surface precipitation algorithm using surface-independent precipitation signatures as index into empirical database.

4.0 ALGORITHM INFRASTRUCTURE

The code to ingest T_bs and ancillary files, perform quality control, assign surface types and decide on channel selection will be written and maintained at Colorado State University in Fort Collins, Colorado, USA. The architecture will be open to all team members as well as outside parties. We will use the input and output sections of this ATBD as a living document that is intended not only for the user of the precipitation product, but also for the algorithm developers to convey precise information about procedures, methods and formats. The code will strive to be machine independent but will first order everyone on the algorithm development team to match the architecture planned by the PPS.

The algorithm itself consists of Fortran 90 code that self-contained in the Algorithm directory. All parameter fields and static databases must be accessible from this directory location as well as the dynamic ancillary data fields. These include the daily SST and Sea-Ice fields read in from NOAA's Reynolds High-resolution Analysis (Reynolds *et al.* 2006) and the various Atmospheric background fields read in from *ECMWF*. (Note that the ATBD uses *ECMWF* as a proxy only. The final model will be selected for processing based upon operational availability as well as consensus with the other algorithm teams. *ECMWF* is therefore in italics).

These files are located in their individual directories that include code to convert the Reynolds and *ECMWF* formats into the format required by the algorithm. It is assumed that PI processing would have these files in place within the directories whereas the real time processing would make this a two step process – starting with the acquisition of the external data files and then running the algorithm in sequence.

Sensor specific landmasks are created by ingesting the land/sea data from the MODIS / SeaWIFS / Ocean Color landmask (reference). This was initially generated in 1993 and based on the World Vector Shoreline (WVS) database. This database did not include any inland waterways, so at that time, those areas were simply flagged as land. In October 1997, shortly after the SeaWiFS launch, the file was modified to include inland waterways, based on the World Data Bank (WDB) information. The final result is a 1/128th degree global grid which specifies either land or water. This is the data file from which the GPM landmasks are derived. The landmask files will be a $1/16^{th}$ degree grid, derived at two different nominal sensor footprints - 19GHz and 85GHz. If the $1/16^{th}$ degree gridbox doesn't have 100% land or ocean, the capability to examine finer resolution land/ocean specifications down to 2 km will be made available.

4.1 ALGORITHM INPUT

The algorithm requires Level 1C brightness temperatures from each sensor.

4.1.1 Ancillary Files

These include individual sensor landmasks, profile databases, elevation, and seasonal emissivity

4.1.2 Reynolds SST and Sea-Ice

Daily global fields of SST and Sea-Ice (downloaded once per day from NCDC)

4.1.3 *ECMWF* Forecast

Various fields are necessary in near-real time which includes profile temperature and humidity.

4.2 PROCESSING OUTLINE

4.2.1 Preprocessor

The preprocessor is the interface between the orbital data files and the GPM PA. The GPM sensor specific preprocessors read from the L1C HDF files and create the standard input file format. The preprocessor includes pixel T_bs, latitude/longitudes, sensor specifications, and names and locations of the ancillary data directories, and profile

databases for land, ocean, and coast – everything the GPM PA needs to run the rainfall retrievals. The preprocessor will also have the task of convolving or de-convolving the channels to two standard footprint sizes (19GHz and 85GHZ) as well as geographically and temporally matching the pixels for offsets due to pointing geometries.

4.2.2 GPM Processing Algorithm

The GPM PA starts by reading the Standard Input file produced from the preprocessor. The sensor T_bs data, all the sensor specifics, and ancillary data locations are input from the pre-processor files. The first task is to assign all the ancillary data to each individual sensor pixel which includes SST, sea-ice, and NWP parameters including freezing heights, total precipitable water, and temperature and moisture profiles, including the total precipitable water. Then assign a surface type based on land masks, sea-ice, vegetation type, and emissivity.

The next step is the actual Bayesian rainfall and hydrometeor profile retrieval, where the observed sensor T_bs are 'matched' to the profile databases. Finally, all the retrieved parameters including a code for the best hydrometeor profile matches are output to a native formatted file.

4.2.3 GPM Format Converter

Changes GPM PA native output format to NetCDF, HDF, HDF-EOS, or whatever is required.

4.3 FLOW DESCRIPTION

Processing flow concepts are shown below. Sensor and spacecraft information is read in by the preprocessors while other ancillary information is added. This creates the intermediary 'Standard Input File' which is read in by the GPM Processing Algorithm. Global fields of other ancillary data are also read into the GPM PA where the retrievals are performed and output to a native output file. Finally, this file can be converted into various output file formats.

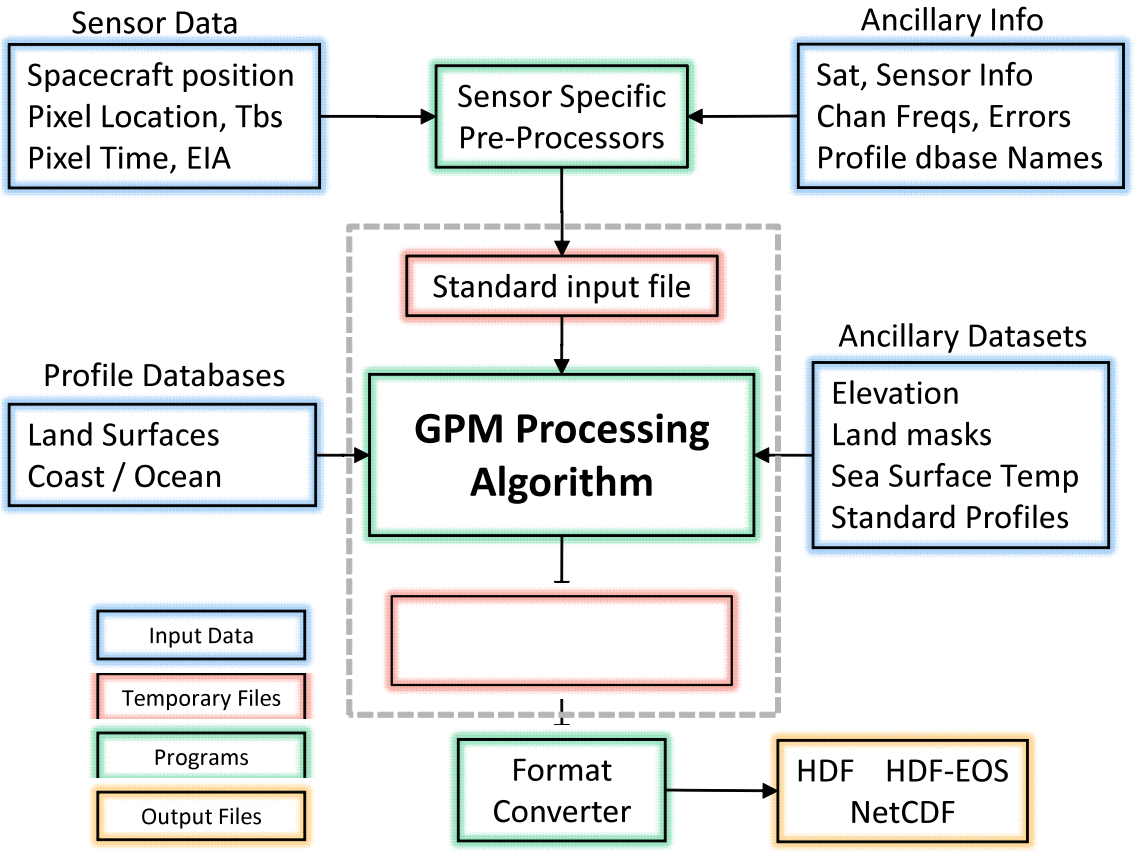

Diagrammatic overviews of the processing concepts for the GPM Processing Algorithm are presented above.

4.4 ALGORITHM OUTPUT FORMAT

Whether in the native, HDF, or NetCDF formats, the output parameters will be equivalent. The following format description is for the GPM native output binary format file.

4.4.1 Orbit Header Record - at beginning of each file

Satellite
Sensor
Pre-processor Version
Algorithm Version
Empirical Database Filename
Ocean Database Filename
Land Database Filename(s)
Original Input Filename
Structure Flag (profiles included?)
File Creation Date/Time
Granule Start Date/Time
Granule Number
HgtLayerTop(28 layers)
Missing Data Value
Number of Scans
Number of Pixels/Scan

4.4.2 Hydrometeor Profile Database

Clusterprofile : Profile database partitioned by species and freezing height. There are a 1300 possible unique profiles for each species.

- Cluster(nspecies=6, nfrzhgts=13, nlayers=28, nclusters=100)

4.4.3 Scan Header Record – at beginning of each scan

Scan Date/Time (yr,mon,day,hour,min,sec)
Spacecraft latitude
Spacecraft longitude
Spacecraft altitude (km)

4.4.4 Pixel Data Record – for each pixel in Scan

latitude, longitude
pixel Status
surface Type
quality Flag
land Database Expansion Index
ocean Database Expansion Index
sun Glint Angle
freezing Height
surface Temperature
surface Precipitation
precipitation Diagnostics
- convective precip
- surface rain
- probability of precip
- maximum likelihood
- sigma
- skewness

land Surface Parameters
- vegetation type
- vegetation cover
- soil moisture
- TDB

ocean Surface Parameters
- cloud liquid water
- total precipitable water
- wind speed

cloud Water Path
rain Water Path
ice Water Path
profile Number
profile Scale (nspecies=6)
profile Freezing height index
comments

4.4.5 Orbit Header Record Variable Description

Satellite

Generally this is a 3 letter internal code for the satellite which produced the data. GPM, MTP, AME, F08, F10, F11, F13, F14, F15, F16, F17, F18, TMI, WND

Sensor

Satellite Sensor, currently:
GPI, MAD, AMSR-E, SSM/I, SSMIS, TRMM, WINDSAT

Pre Processor Version

GPM Pre-Processor version number

Algorithm Version

GPM Processing Algorithm Version which produced the output file.

Empirical, Ocean, and Land Databases

File names of the various profile databases. May be expanded to include multiple databases with each surface type.

Original Input Filename

File Name of the original; input data file.

Structure Flag

Flag defining whether GPM PA was run with vertical profiles of the hydrometeors. No structure = 0, with vertical structure = 1.

Creation Date/Time

Start date and time of file creation. Defined as the date/time structure which holds six integer*2 values - year, month, day, hour, minute, second.

Granule Start Date/Time

Start date and time of first scan in file. Defined as the date/time structure which holds six integer*2 values - year, month, day, hour, minute, second.

Granule Number

Generally this is defined as the satellite orbit number since launch.

Hgt Layer Top

Height of the top of each 28 layers of GPM PA in kilometers (km). These are defined every 0.5 km up to 10 km, then every kilometer after that up to 18 km. Values are: 0.5, 1., 1.5, 2., 2.5, 3., 3.5,4.,4.5,5.,5.5, 6.,6.5,7., 7.5, 8., 8.5, 9., 9.5,10., 11., 12., 13., 14.,15., 16., 17., 18.

Missing Data Value

Value of the floating point missing data.

Number of Scans

Number of scans in the file

Number of Pixels per Scan

Number of pixels per scan for this sensor

Comments

Available open space for various comments and spare bytes, and error messages

4.4.6 Pixel Data Record Variable Descriptions

Latitude, longitude

Pixel latitude and longitude.

pixel Status – a full list of these can only be created once the algorithm is finalized.

If there is no retrieval at a given pixel, pixelStatus explains the reason.

0 : Valid pixel
1 : Boundary error in landmask
2 : Boundary error in sea-ice check
3 : Boundary error in sea surface temperature
4 : Invalid time
5 : Invalid latitude/longitude
6 : Invalid brightness temperature
7 : Invalid sea surface temperature
8 : No retrieval due to sea-ice over water
9 : No retrieval due to sea-ice over coast
10 : Failure in land rain retrieval – no match with database T_bs
11 : Failure in ocean rain - no match with database profile T_bs

surface Type

Surface type codes are as follows:

10 : Ocean
11 : Sea ice
12 : Partial sea ice
15 : Inland water
100 - 200: land surface groupings (by emissivity or other catagories)

quality Flag

qualityFlag indicates a generalized quality of the retrieved pixel. Values follow:
Ocean Algorithm:

High: Good retrieval (uses only entries from apriori database)
Medium: Retrieval used extended parts of the database
Low: Retrieval used excessive search radius to find matches in profile database (see Database Expansion Index)

1 : Highest quality – (use it!)
2 : Medium quality (use with caution)
3 : Low quality (recommended qualitative use only)

land Database Expansion Index

This Value is the expansion factor of the profile search radius in the land profile database beyond the search nominal range. If there is fewer than the minimum number of profiles in the selected database boundaries, then the search radius is expanded.

ocean Database Expansion Index

Expansion of the search radius of profiles in the *a-priori* ocean database beyond the initial SST and TPW search range. The individual pixels TPW and SST are used to retrieve a group of pixels from the database. If there are fewer than 1000 profile clusters found, the search radius is expanded. Valid values are:

0 : Default search radius used
1 : Search radius expanded by +/- 1 mm (TPW) and +/- 1 degree (SST)
N : Search radius expanded by +/- N mm (TPW) and +/- N degrees (SST)

sun Glint Angle

Conceptually, the angle between the sun and the instrument view direction as reflected off the Earth's surface. More specifically, define a Sun Vector from the viewed pixel location on the earth ellipsoid-model surface to the sun. Also define an Inverse Satellite Vector from the pixel to the satellite. Then reflect the Inverse Satellite Vector off the earth's surface at the pixel location to form the Reflected Satellite View Vector. sunGlintAngle is the angular separation between the Reflected Satellite View Vector and the Sun Vector. When sunGlintAngle is zero, the instrument views the center of the specular (mirror-like) sun reflection. Values range from 0 to 180 degrees.

freezing Height

The height, in meters, of the 0^{o}C isotherm above the earth ellipsoid.

Surface Temperature

Land or Ocean surface temperature. Land temperatures will be recovered from the forecast models. Ocean temperatures are from the 0.5^{o} daily Reynolds SST dataset. Values in degrees K.

surface Precipitation

The instantaneous precipitation rate at the surface. Check pixelStatus for a valid retrieval. Values are in mm/hr.

precipitation Diagnostics

- convective Precipitation

The instantaneous convective precipitation rate at the surface. Check pixelStatus for a valid retrieval. Values are in mm/hr.

- surface Rain

The instantaneous rain rate (liquid portion of precipitation) at the surface for each pixel. Check pixelStatus for a valid retrieval. Values are in mm/hr.

- probability of Precipitation

A diagnostic variable, in percent, defining the fraction of raining vs. non-raining Dbase profiles that make up the final solution. Values range from 0 to 100%.

- maximum Likelihood, Sigma, Skewness

Statistical description of the precipitation retrieval for this pixel.

land Surface Parameters

- vegetation type
- vegetation cover
- soil moisture
- other parameters TDB

ocean Surface Parameters

- cloud liquid water
- total precipitation water
- wind speed
- other parameters TDB

cloud Water Path, rain Water Path, Ice Water Path

Total cloud liquid water, total rain water and total cloud ice in the column.

profile Number, profile Scale, **profile Freezing Height Index**

Profile Number, Profile Scale, and Profile Freezing Height Index of the pixels profile in the corresponding cluster array. See 'Hydrometeror Profile Recovery' description below.

4.5 HYDROMETEOR PROFILE RECOVERY

In order to recover hydrometer profile values of a single pixel, use the profileNumber, profileScale and profilefreezingHeightIndex parameters, select your species and loop over the levels, and pluging these indices into the 'clusterprofile' array. Where:

S = species(1-6)
- 1 = cloud water content
- 2 = rain water content
- 3 = cloud ice content
- 4 = snow water content
- 5 = graupel water content
- 6 = latent heat

F = profileFreezingHeightIndex

L = profile level (1-18). The pop of each level specified in HgtLayerTop
P = profileNumber

Pixel value = profileScale(S) * cluster(S,F,L,P)

5.0 ASSUMPTIONS AND LIMITATIONS

5.1 ASSUMPTIONS

TBD

5.2 LIMITATIONS

TBD

6.0 PLANNED ALGORITHM IMPROVEMENTS

Transition to later algorithms with the GPM database: For the first GPM-based *a-priori* database, the radiometer algorithm team will create an empirical database using DPR observed precipitation and GMI observations. Techniques that have been developed jointly with the X-cal team will be used to translate the observed GMI T_bs to equivalent T_b that would be observed by other constellation radiometers. This can be done quickly and will ensure that a good product is available from the radiometers soon after launch. Future versions will rely on physically constructed solutions from the "combined algorithm" team. Physical solutions not only ensure consistency between radar and radiometer, but the retrieved geophysical parameters also ensure that the computed T_b for the constellation radiometers is fully consistent with the *a-priori* database. Since the "combined algorithm" product becomes the *a-priori* database for GMI as well as the radiometer constellation, the radiometer algorithm should always be implemented 6 months after the reprocessing of the "combined algorithm." This represents a departure from the TRMM model where all algorithms are reprocessed simultaneously.

The transition to "fully physical" retrievals: The first database as described above is empirical in nature. By this we understand that a radiative transfer computation using the retrieved rainfall profiles from DPR do not necessarily yield the T_b observed by GMI. The reasons for the differences can be many, including; incorrect assumptions about drop size distributions, cloud water contents, ice microphysics, or surface properties. In some cases, such as tropical oceans, we have already developed techniques to adjust retrieved parameters so as to be simultaneously consistent with radar and radiometer observations on TRMM. These regions will be quickly transitioned (in the first reprocessing) from

empirical to physical within GPM as well. The combined algorithm, however, will not always be able to create physically consistent solutions between DPR and GMI. An example is a complex coast line where emissivity is not known or calculable. The combined algorithm in this case will use only DPR to create a solution, leaving the *a-priori* database needed by the radiometer to be empirical. Because of this, the radiometer algorithm plans on a phased approach, starting with an empirically constructed *a-priori* database and transitioning this database to a physical one as we understand specific surfaces. The degree to which various surfaces are physically understood is shown below.

Emissivity models: Over oceans, good emissivity models exist that allow "combined retrievals" to produce physically consistent geophysical parameters. Over land, there are some surfaces where good knowledge exists (e.g. rain forests) while others (e.g. semi-arid regions) still require significant work before a truly physical model of the emissivity can be constructed. In the GPM combined algorithm, two steps are defined. The first step requires only co-variances of the emissivities among channels. When these covariances are well defined and reduce the emissivity problem to one or two degrees of freedom, then physical databases can be constructed that retrieve these one or two degrees of freedom. This will be done first as different investigators provide guidance on the best way to define these degrees of freedom for individual surfaces. From an algorithm point of view, this is the only step that is required. From a GPM science point of view, we want to further know how the free parameters are related to geophysical parameters that can then be assimilated into Land Surface Models (LSMs). Conversely, if the relationship between emissivity and emissivity covariance and land surface parameters is known, then LSMs can be used to limit the degrees of freedom that have to be retrieved with respect to the surface in much the same way that a weather forecast model can already be used to specific atmospheric temperature structure. First, in order to use the useful co-variances among channels and then the entire LSM, the retrieval algorithm must be able to identify the specific surfaces of applicability. We will track the portion of the globe that uses these physical methods versus the default empirical methods as part of the algorithm development.

REFERENCES (Incomplete)

Aires, F., C. Prigent, F. Bernardo, C. Jimenez, R. Saunders, and P. Brunel, *A Tool to Estimate Land Surface Emissivities in the Microwaves (TELSEM) for use in numerical weather prediction schemes.* Q. J. Royal Meteor. Soc. , 2010, in review.

Aires, F., F. Bernardo, H. Brogniez, and C. Prigent, *Calibration for the inversion of satellite observations,* J. of Applied Meteorology, 2010, in press.

Backus, G., and F. Gilbert, 1970: Uniqueness in the inversion of inaccurate gross earth data, *Philos. Trans. Roy. Soc. London*, A266, 123–192.

Berg, W., T. L'Ecuyer, and C. Kummerow, 2006. Rainfall climate regimes: The relationship of regional TRMM rainfall biases to the environment, *J. Appl. Meteor. Climatol.*, **45**, 434–454.

Hollinger, J.P. 1989: *DMSP Special Sensor Microwave/Imager Calibration/Validation*. Final Report, Vol. I., Space Sensing Branch, Naval Research Laboratory, Washington D.C.

Kummerow, C., W. Barnes, T. Kozu, J. Shiue and J. Simpson, 1998. The tropical rainfall measuring mission (TRMM) sensor package, *J. Atmos. Oceanic Technol.*, **15**, 809–817.

Kummerow, C., W.S. Olson and L. Giglio, 1996. A simplified scheme for obtaining precipitation and vertical hydrometeor profiles from passive microwave sensors, *IEEE, Trans on Geoscience and Remote Sensing,* **34**, 1213-1232, doi: 10.1109/36.536538.

Lorenc 1986.

Prigent, C., E. Jaumouille, F. Chevallier, and F. Aires, *A parameterization of the microwave land surface emissivity between 19 and 100 GHz, anchored to satellite-derived estimates,* IEEE Transaction on Geoscience and Remote Sensing , 46, 344-352, 2008.

Prigent, C., F. Aires, and W.B. Rossow, *Land Surface Microwave Emissivities over the Globe for a Decade,* Bulletin of the American Meteorological Society, DOI:10.1175/BAMS-87-11-1573, pp. 1572-1584, Nov. 2006.

Rapp, A., M. Lebsock, C. Kummerow, 2009: On the Consequences of Resampling Microwave Radiometer Observations for Use in Retrieval Algorithms, *J. of Appl. Meteo. and Clim.,* **48**, 2242-2256, doi: 10.1175/2009JAMC2156.1.

Reynolds, R.W., T.M. Smith, C. Liu, D.B. Chelton, K.S. Casey, and M.G. Schlax, 2006: Daily High-Resolution-Blended Analyses for Sea Surface Temperature. *J. Climate,* **20,** 5473- 5496.

Sudradjat, A., N-Y. Wang, K. Gopalan and R. Ferraro, 2011: Prototyping a Generic, Unified Land Surface Classification and Screening Methodology for GPM-era Microwave Land Precipitation Retrieval Algorithms. *Under revision, J. Applied Meteor. and Climat.*